



**HAL**  
open science

## The impacts of Persian Gulf water and ocean-atmosphere interactions on tropical cyclone intensification in the Arabian Sea

Majid Pourkerman, Nick Marriner, Sedigheh Amjadi, Razyeh Lak, Mohammadali Hamzeh, Gholamreza Mohammadpor, Hamid Lahijani, Morteza Tavakoli, Christophe Morhange, Majid Shah-Hosseini

### ► To cite this version:

Majid Pourkerman, Nick Marriner, Sedigheh Amjadi, Razyeh Lak, Mohammadali Hamzeh, et al.. The impacts of Persian Gulf water and ocean-atmosphere interactions on tropical cyclone intensification in the Arabian Sea. *Marine Pollution Bulletin*, 2023, 188, pp.114553. 10.1016/j.marpolbul.2022.114553 . hal-03959955

**HAL Id: hal-03959955**

**<https://hal.science/hal-03959955>**

Submitted on 27 Jan 2023

**HAL** is a multi-disciplinary open access archive for the deposit and dissemination of scientific research documents, whether they are published or not. The documents may come from teaching and research institutions in France or abroad, or from public or private research centers.

L'archive ouverte pluridisciplinaire **HAL**, est destinée au dépôt et à la diffusion de documents scientifiques de niveau recherche, publiés ou non, émanant des établissements d'enseignement et de recherche français ou étrangers, des laboratoires publics ou privés.

This is a postprint version, the definitive version of this paper is :

Pourkerman, M., Marriner, N., Amjadi, S., Lak, R., Hamzeh, M., Mohammadpor, G., Lahijani, H., Tavakoli, M., Morhange, C., & Shah-Hosseini, M. (2023). The impacts of Persian Gulf water and ocean-atmosphere interactions on tropical cyclone intensification in the Arabian Sea. *Marine Pollution Bulletin*, 188, 114553. <https://doi.org/10.1016/j.marpolbul.2022.114553>

---

## **The impacts of Persian Gulf water and ocean-atmospheric interactions on tropical cyclone intensification in the Arabian Sea**

Majid Pourkerman <sup>\*1</sup>, Nick Marriner <sup>\*2</sup>, Sedigheh Amjadi <sup>1</sup>, Mohammadali Hamzeh <sup>1</sup>, Gholamreza Mohammadpor <sup>1</sup>, Hamid Lahijani <sup>1,3</sup>, Morteza Tavakoli <sup>1,4</sup>, Christophe Morhange <sup>5</sup>Razyeh Lak<sup>6</sup>

1- Iranian National Institute for Oceanography and Atmospheric Science (INIOAS), Tehran, Iran

2- CNRS, ThéMA UMR 6049, Université de Bourgogne Franche-Comté, MSHE Ledoux, Besançon, France

3- Eurasian Institute of Earth Sciences, Istanbul Technical University (ITU), Ayazaga, 80626 Istanbul, Turkey

4- Department of Geography and Rural Planning, Tarbiat Modares University, P.O. Box 14115-175, Tehran, Iran

5- Aix Marseille Univ, CNRS, IRD, INRAE, CEREGE, Aix-en-Provence, France

6- Research institute for earth sciences, geological survey of Iran, P.O.Box 13158-1494, Tehran, Iran

\* Corresponding authors

### **Abstract**

During the last two decades, the number of tropical cyclone (TC) events in the Arabian Sea has increased dramatically, causing severe human and economic damage in Oman, Iran and Pakistan. Within this context, Gonu, Phet and Shaheen were the Arabian Sea's most destructive TCs on record, leading to a total of 6.07 billion USD in damages and 159 fatalities. Previous studies have mainly focused on atmospheric, sea surface temperature (SST) and anthropogenic impacts of TC generation and intensification. By contrast, oceanographic currents, Persian Gulf water outflow and the role of ocean-atmospheric interactions on the distribution of outflow water into the Arabian Sea, and their impacts on the TC intensification, are poorly understood. In order to address this issue, we use historical TC records, satellite data, atmospheric and oceanographic models to shed new light on the relationship between Persian Gulf water outflow and ocean currents on TC intensification in the Arabian Sea. The results demonstrate that water outflow depths are controlled by wind stress and upwelling intensity. Increased upwelling events due to the poleward movement of the monsoon belt have led to an increase in upper ocean salinity and heat content. Rapid TC intensification has increased noticeably since 2007 and more than 72% of cyclones have reached category 3 or more. We find that TC intensity is controlled by warm and saline (> 36.6 PSU) water distribution patterns, mediated by eddy and jet currents. Rapid intensification of pre-monsoon TCs occurred by tracking to the north and northwest, with most landfalls occurring during this period. Post-monsoon TCs generally affect the center and the southwest of the Arabian Sea. The TC risk manifests an increasing trend since 2007, therefore education programs via international platforms such as the International Ocean Institute (IOI) and UNESCO are required for the countries most at risk.

**Keywords:** *Tropical cyclone, Ocean-atmosphere interaction, Arabian Sea, SST, Eddy current, natural hazard.*

## 1. Introduction

Tropical cyclones (TCs) are amongst the most devastating natural hazards worldwide. They have led to considerable economic and humanitarian damage in densely populated coastal areas, including the degradation of industrial and fishery infrastructure (ports, desalination plants, petrochemical facility and etc.) and destructive winds and flashfloods on coastal plains (Wang and Oey 2008; Han et al. 2012; Sun et al. 2013; Mei et al., 2015; Zhang et al. 2016). According to the World Meteorological Organization, the world's deadliest tropical cyclone during last 50 years was Cyclone Bhola, which formed in the south of the Bay of Bengal and hit Bangladesh on the 12<sup>th</sup>-13<sup>th</sup> November 1970. Nearly half a million people were killed due to the large storm surge, which overwhelmed tidal flats and low-lying islands in the Bay of Bengal. The Orissa super cyclone in 1999, and Cyclone Nargis in 2008, caused around 238,000 deaths in Bangladesh and Myanmar (Singh et al., 2001).

TC genesis is controlled by four physical processes: atmospheric conditions (low-level cyclonic vorticity, less vertical wind shear, moisture at mid-tropospheric level), internal TC dynamics, Coriolis forces and underlying boundary conditions (Chen and Ding, 1979; Gray, 1979; Emanuel et al., 2004). The underlying boundary conditions, such as sea surface temperature (SST) and sufficiently mixed deep water are the most important factors for TC intensification (Jaimes et al., 2011; Yablonsky and Ginis, 2012; Yan et al., 2017; Lavender et al., 2018; Sun et al., 2019). The TC's energy source is heat transfer from the ocean surface; this heat is used to strengthen a cyclonic disturbance into an intense vortex. TC intensification is correlated with the 26.5°C isotherm depth and upper ocean heat content (Palmen, 1948; Williams, 2013; Shay and Brewster, 2010; Ackerman and Knox, 2015).

TCs occur in the southwest Pacific, the northeast and northwest Pacific, the North Atlantic, the northern and southern Indian Ocean and Australian Sea basins (Gray, 1979). A recent study on the global distribution pattern of TCs for 1980-2018 demonstrated that the frequency of TCs has decreased over the southern Indian Ocean, the northeast of the Australian Sea and the northwest Pacific. Meanwhile, an increasing trend is observed in the Arabian Sea (AS), the northern Atlantic and central Pacific basins (Murakami et al., 2020). TCs are rare phenomena in the north Indian Ocean and just 6% of global tropical cyclones annually occur in this basin (Singh and Roxy, 2022). The north Indian Ocean basin is divided into the Bay of Bengal (BoB) and the Arabian Sea (AS) basins. The number of TC events in the Bay of Bengal is four times greater than the Arabian Sea. The average TC frequency (Bay of Bengal/Arabian Sea) for the period 1982-2000 was 2.7 events/year and 1.6 events/year between 2001 and 2019. For the recent period, TC duration has significantly increased in the Arabian Sea. The increase in TC frequency and duration in the Arabian Sea has been concurrent with accelerating accumulated cyclone energy during the pre-monsoon (March–April–May) and post-monsoon (October–November) seasons. By contrast, no significant changes in TCs were observed in the Bay of Bengal (Deshpande et al., 2021; Bandyopadhyay et al., 2021).

TC activities in the north Indian Ocean are affected by changes in large scale ocean-atmosphere conditions such as the El Niño Southern Oscillation, the Indian Ocean Dipole (IOD) and the Madden-Julian Oscillation (MJO). During La Niña years, an increase in cyclone frequency and intensity is observed in the north Indian Ocean especially in the Bay of Bengal (Girishkumar et al., 2015; Bhardwaj et al., 2019). Similar to La Niña years, the negative IOD years also have significant effects on cyclone frequency in the north Indian Ocean (Li et al., 2016). During negative IOD years, westerly wind intensified along the equator and led to increased upwelling in the western Indian Ocean and anomalous warmer SST in the eastern tropical Indian Ocean. It creates favorable atmospheric conditions such as enhanced relative humidity, and relative vorticity for cyclone formation in the Bay of Bengal (Mahala et al., 2015). The MJO at the subseasonal scale has significant impacts on TC formation and intensification in the northern Indian Ocean (Singh et al., 2020). MJO is an eastward-propagating band of enhanced convection in the tropical regions with a poleward component in the boreal summer season (Kawamura et al., 2010).

The intensity of the cyclones is significantly affected by mesoscale features such as eddies. The ocean mesoscale eddy is a significant ocean phenomenon that covers 20-30% of the global ocean area (Cheng et al., 2014; Lumpkin, 2016). The mesoscale eddy (ME) circulation system has important effects on surface ocean water temperatures and also on subsurface layers, general circulation and regional climate (Macdonald & Wunsch, 1996; Dong et al., 2014; Zhang, et al., 2014; Yang et al., 2015). Mesoscale eddy energy transfer have positive impacts on TC intensity (Sun et al., 2020). Strong eddy activity exists in the western basin of the Arabian Sea that is similar to eddy-rich regions in the global ocean (Scharffenberg & Stammer, 2010; Rouillet et al., 2014). Eddy activities in the Arabian Sea exhibit strong seasonality that peaks during the summer monsoon season (Trott et al., 2018). Wind stress, the Somali current, the westerly propagating Rossby wave and background currents are all parameters that can further reinforce eddies in the region (Brandt et al., 2002; Trott et al., 2017). Anticyclonic eddies are associated with a warm core and downwelling region and have high Sea Level Anomaly (SLA) and high ocean heat content (Kumar and Chakraborty 2011). Instead, cyclonic eddies with cold cores are associated with upwelling, low SLA and low ocean heat content. In the north Indian Ocean, eddies are created due to the baroclinic instability and coastal currents during pre and post monsoon seasons (Vinayachandran et al., 2005; Kurien et al., 2010). Warm core eddies are more common during the pre-monsoon season than the post-monsoon season (Jangir et al., 2021).

During the last two decades three TCs (Gonu, Phet and Shaheen) have reached the Gulf of Oman, leading to heavy damage in Iran, Oman and Pakistan. The Gulf of Oman is the only maritime entrance into the Persian Gulf (Fig 1), a region which exports approximately 18.2 million barrels of oil per day. Several important cargo and fishery ports also exist on the Omani and Iranian coasts that are vital for the regional economy. The increasing number, intensity and duration of TC events in the Arabian Sea and the Gulf of Oman could accentuate maritime risks and economic damage at both local and global scales.

The aim of this study is to evaluate the impacts of the Persian Gulf water outflow and ocean-atmospheric interaction on TC generation and intensification. In this study we employ satellite data, model reanalysis and statistical analyses to study destructive TC (Gonu, Phet and Shaheen) intensification in the Arabian Sea.

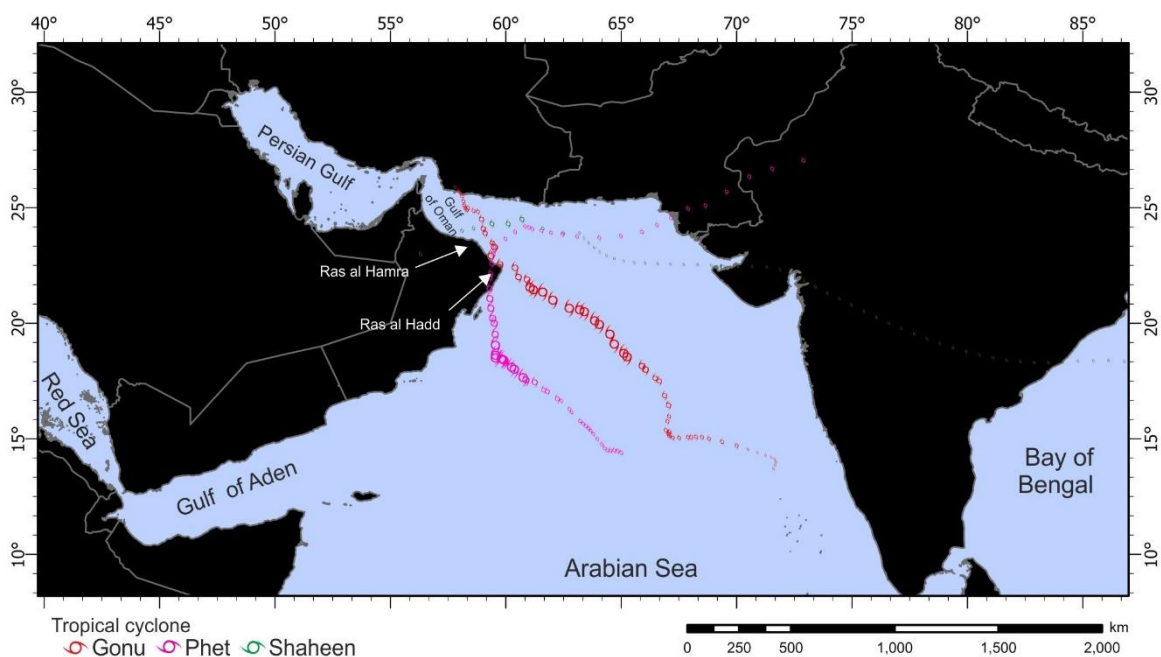


Figure 1: Regional map of the study area and tracks of the studied TCs

## **2. Oceanographic currents**

### *2.1. Persian Gulf water outflow*

The Persian Gulf is a semi-enclosed basin with an average depth of 35m. It opens onto the Gulf of Oman via the Strait of Hormuz. The Strait of Hormuz is 110m deep; in contrast, the Gulf of Oman is a deep sea with a maximum depth of 3,000m. Water circulation in the Persian Gulf is mainly controlled by the northwesterly Shamal winds and density gradients (Pous et al. 2013). Low precipitation and high evaporation (1.84 m/year) mean that Persian Gulf water is hypersaline (Xue and Eltahir, 2015). Water exchange between the Persian Gulf and the Gulf of Oman is an inverse-estuary circulation, so that Indian Ocean freshwater enters the Gulf near the surface while saline and denser water is exported to deeper layers in the Gulf of Oman (Johns et al., 2003). The volume of water exchange varies seasonally, with denser water (colder and more saline) forming in the autumn and winter on the southern Arabian coast before being exported during the winter and spring (21°C and 40.8 PSU). In contrast, the temperature and salinity of the outflow water in summer are about 25°C and 39.3 PSU (Pous et al. 2004a; Lorenz et al., 2019). The density of the outflow water decreases due to mixing with the surrounding water in the Strait of Hormuz and at Ras al Hamra. The Persian Gulf water is reached about 250m depth along the Oman coast. The geography of outflow water has a complex spatial pattern. In summer, it outflows along the Omani coast down to Ras al Hadd and then bifurcates south-eastwards. Meanwhile, the Persian Gulf water progresses offshore at Ras al Hadd and flows to the southern Omani coast in the winter (Pous et al. 2004b).

### *2.2. Gulf of Oman and Ras al Hadd dipolar eddy*

Ras al Hadd constitutes the eastern tip of the Arabian Peninsula. The Ras al Hadd dipole is associated with an anticyclonic eddy to the southeast and a cyclonic eddy to the northeast that forms in the summer and breaks up at the end of autumn (Ayouche et al., 2021). Along the axis of this dipole, an intense Ras al Hadd jet flow exists. The Ras al Hadd jet is an integral part of the east Arabian current which is the northward extension of the Somali current. During the summer monsoon (May to September), it becomes the northern edge of the east Arabian current and advects primarily upwelled cold water along the Oman coast. During the inter-monsoon period when the wind system reverses warm current is rapidly established and advects surface coastal waters of the Gulf of Oman offshore (Böhm et al., 1999). 3D structural analysis of the Ras al Hadd oceanic dipole shows that the cyclonic eddy is a surface-intensified result of interaction with the atmosphere and favors the shallower eddy while the anticyclonic eddy is intensified on the subsurface (Bennani et al., 2022).

Long-term analysis of surface eddies in the Gulf of Oman shows a largely similar evolution. In September, before each spring dipole, the circulation in the Gulf of Oman is generally cyclonic. An anticyclonic circulation with westward movement is observed in winter. The anticyclonic eddy reaches Ras al Hamra during February to March. Through July to August, the anticyclone current weakens and circulation becomes cyclonic in autumn and early winter. The mesoscale eddy in the northern Arabian Sea plays an important role in the circulation and distribution of Persian Gulf water. The warm and salty outflow water recirculates through the Gulf of Oman and flows eastwards along the Iranian and Pakistani coasts via geostrophic currents (L'Hégaret et al., 2013).

## **3. Material and methods**

### *3.1. TC tracks*

In this study, we used the International Best Track Archive for Climate Stewardship (IBTrACS) dataset to track TCs in the Arabian Sea basin. IBTrACS contains a time series of storm positions from forecasting agencies around the world, including information on the location and intensity of TCs at 6-hour intervals (Knapp et al. 2010). The TC categories are classified according to wind speed: category 0 (63 - 118 km/h), category 1 (119 - 153 km/h), category 2 (154 - 177 km /h), category 3 (178 - 208 km/h), category 4 (209 - 251 km/h) and category 5 ( $\geq 252$  km km/h). Tropical cyclone lifecycles were tracked using high-rate rectified SEVIRI IR10.8  $\mu\text{m}$  Image of Meteosat-8 data available since

September 2020. In addition, IBTrACS includes information about Sea Level Pressure (SPL) from different sources. In this study we used World Meteorological Organization (WMO) data for tracking SPL changes along the TCs' core tracks.

### 3.2. Satellite and reanalysis data

Long-term SST changes were calculated using average SSTs at 20-year intervals for the period 1860-2021. The data were extracted from the International Comprehensive Ocean-Atmosphere Data Set (ICOADS) for the area 8-25.5°N to 50-74°E. The ICOADS data are provided by the NOAA/OAR/ESRL PSL, Boulder, Colorado, USA (<http://www.esrl.noaa.gov/psd/>). We also employed 0.25×0.25 degree daily Optimum Interpolation Sea Surface Temperature (OISST) based on AVHRR (Advanced Very High-Resolution Radiometer) for the SST anomaly changes before, during and after the Gonu, Phet and Shaheen tropical cyclone events. The OISST data derives from different platforms such as satellites, buoys, ships, and Argo floats to improve the accuracy and bias corrections (Reynolds et al., 2007; Huang et al., 2021).

Daily average data of the NCEP/NCAR reanalysis multi-pressure level model (Omega, geopotential height, U/V winds) with 2.5 degree × 2.5 degree resolution was employed to assess atmospheric instabilities before, during and after the studied TC events. In this study, we used vertical velocity, pressure gradient force, wind speed and direction for the 850 hPa and 500 hPa pressure levels.

Horizontal surface current data are based on the Ocean Surface Current Analysis Real-time (OSCAR) model that is developed by Earth Space Research (ESR). 5-day resolution current velocity is estimated by surface vector wind, sea surface height and SST. The formulation of the model in 1/3 degree grids combines geostrophic, Ekman and Stommel shear dynamics and surface buoyancy gradients used for complementary terms. Daily Eddy Kinetic Energy (EKE) was used to calculate the kinetic energy of the time-varying component of the velocity field (including coherent mesoscale eddies and large-scale motions), obtained from National Remote Sensing Centre/Indian Space Research Organization (NRSC/ISRO) data base (<https://bhuvan.nrsc.gov.in>).

Changes in salinity and temperature vertical profiles (0-150m and 0-600m) and mean salinity changes for the depth 0-50 m for the selected time intervals were studied by Multi Observation Global Ocean ARMOR3D L4 analysis (Guinehut et al., 2012; Mulet et al., 2012) generated using the E.U. Copernicus Marine Service Information. The model has a spatial resolution of 1/4 degree down to 50 m depth.

The upper ocean heat content was employed to assess long-term changes in the eddy zone of the Gulf of Oman. The data were downloaded from the NOAA National Center for Environment Information (NCEI) database.

All of the long-term data were extracted for the tropical cyclone seasons. The reanalyzed data are available in NetCDF4 format. Data were extracted using ArcGIS pro ver.2.5.

### 3.3. Statistical analysis

Statistical analyses were performed using Origin pro 2021. All the ocean and atmospheric trends were calculated using polynomial and linear models (lowest standard deviation,  $P_{\text{value}} < 0.001$ ; the  $R^2$  is mentioned on each graph). The graphs show marine-atmosphere condition 3 days before, during and after each studied TC event. Changes in the long-term SST trends (1900-2021) were calculated by linear models for each extracted pixel value and mapped according to the regression slope scores. Daily salinity-temperature profiles were created according to the TCs central path. Long-term (1983-2021) salinity-temperature profiles were generated along the transect from the Strait of Hormuz to Ras al Hadd.

A Principal Component Analysis (PCA) was performed to evaluate TC risk related to Persian Gulf water outflow. PCA analysis was employed for long-term extracted data of SSTA and the upper ocean heat content of the Gulf of Oman, Ras al Hadd eddy core and SSTA at the upwelling zone during

tropical cyclone seasons. Also, long-term wind speed west of the Arabian Sea was considered. The first axis (PCA-axis 1) which carries maximum variance was extracted and plotted with the large-scale atmospheric system (ENSO and IOD). The strongest TCs in the west of the Arabian Sea are loaded by maximum positive PCA-axis 1 scores.

## **4. Results**

### *4.1. Long-term SST changes and TC frequency*

We compared long-term trends in SSTs with TC frequency and intensity in the Arabian Sea for 1900-2021 (Fig 2A). Three important upwelling zones are defined in the Arabian Sea (Pakistan, Oman and Somali) and SST trend changes were plotted for TC seasons (Fig 2B).

During the 1900-1920 time interval, minimum SST is observed at upwelling zones (Somali, Oman and Pakistan coasts) and in the Gulf of Oman (<25 °C to 25.5 °C). East Arabian currents advect cold water along the upwelling zones during the summer and winter monsoons when SST in the Gulf of Oman was low. The period between 1920 and 1980 manifests increasing SST in the eastern Arabian Sea, Gulf of Aden and the Gulf of Oman. During this period, SST in the upwelling zones had increased. This trend continued through 1941-1960 and 1961-1981. SST shows an accelerating trend west and north of the Arabian Sea due to an increase in temperature in the Gulf of Oman when it attained 27.5-28°C. Increasing water temperature in the Gulf of Oman had negative impacts on cold water advection by the east Arabian current during winter and the inter-monsoon seasons. As a result, average SST increased in the north and west of the Arabian Sea (Fig 1A). For the period 1981-2000, SST in the Somali and Pakistan upwelling zones attained 27 °C and 26-26.5°C on the Oman coast. Concurrently, average SST in the Gulf of Oman reached 28°C and 28.5°C in the East Arabian Sea. ARB 01 occurred during the pre-monsoon TC season and it was the first TC that exceeded category 1 in the Arabian Sea (Fig 2).

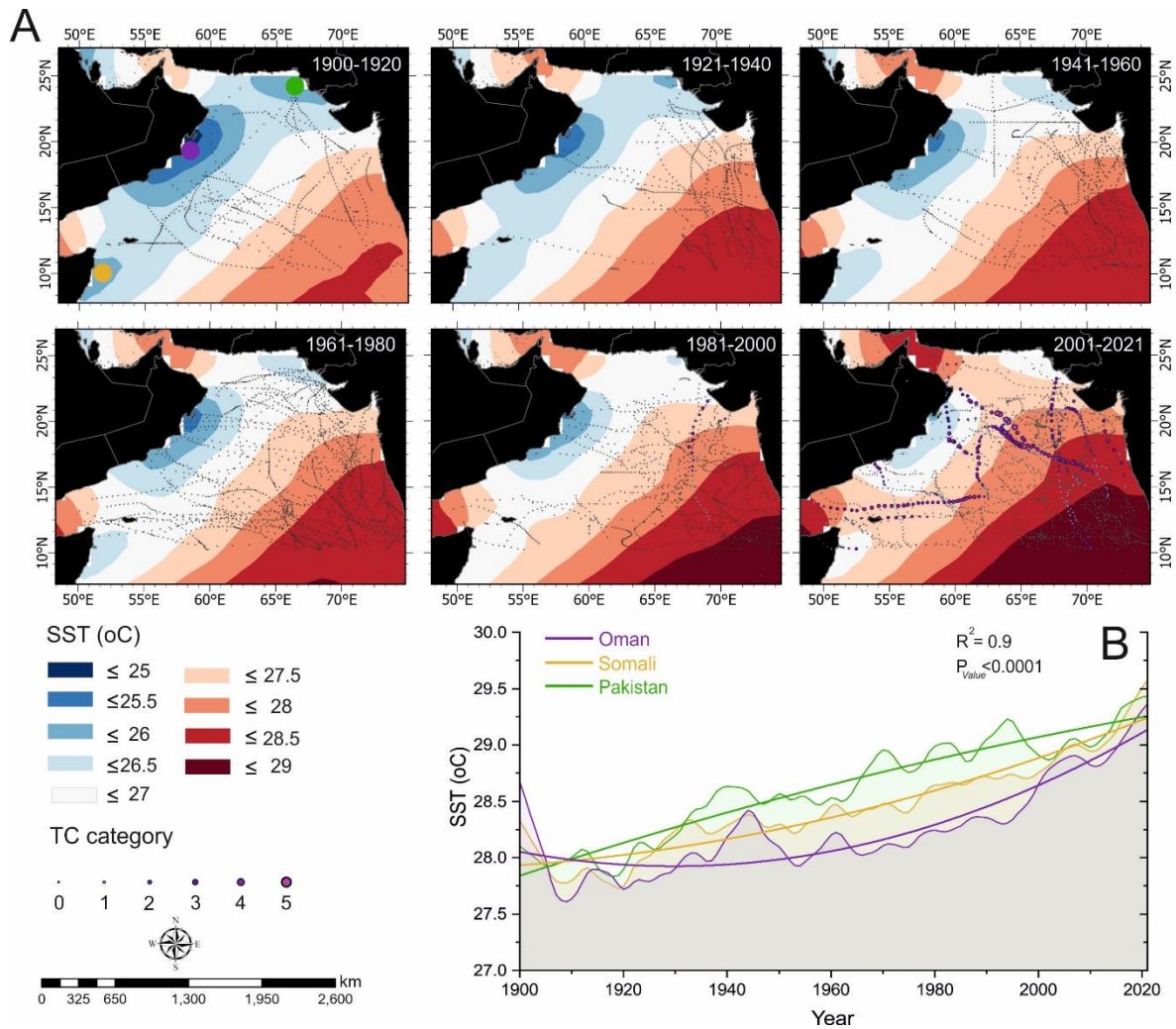


Figure 2: A) Long-term SST changes and TC events from 1900 to 2021. B) The sea surface temperature changes in the major upwelling zones on the Somali, Oman and Pakistan coasts during the cyclone season. Polynomial models (order 5,  $P_{value} < 0.001$ ) were employed to emphasize the long-term trends.

Between 2001 and 2021 increasing SST was observed across all basins (Persian Gulf, Gulf of Adan and Gulf of Oman). The mean SST in the Gulf of Oman and the Gulf of Aden reached 28.5 °C. SST in the Oman upwelling zone attained 26.5 to 27°C, the highest recorded SST since 1900. The linear model of long-term SSTs (1900-2021 monthly data) highlights rising trends for all basins. Maximum SST is recorded in the Gulf of Oman and at Ras al Hadd ( $2.9 \times 10^{-5}$ ), areas under the influence of Persian Gulf outflow (warm and salty water) and mesoscale eddies. Meanwhile, minimum SST changes were recorded east of the Arabian Sea, where maximum heat advection occurred during strong storms and TC events (Fig 3).

Average SST in the Arabian Sea during the period 2000-2021 (26-29 °C) was favorable to TC genesis. As a result, the frequency of TCs increased and the number of strong TCs grew dramatically. The number of TCs exceeding category 1 during the post-monsoon phase was 11, while 6 TCs occurred during the pre-monsoon period. The pre-monsoon TCs generally have a northwest tracking direction and four of them made landfall over Oman (Gonu, Phet, Mekunu) and Pakistan (Tauktae). The post-monsoon TCs generally affected the center and the southwest of the Arabian Sea. Tropical cyclone Shaheen was the only post-monsoon TC that made landfall on the Oman coast (see Fig A1).

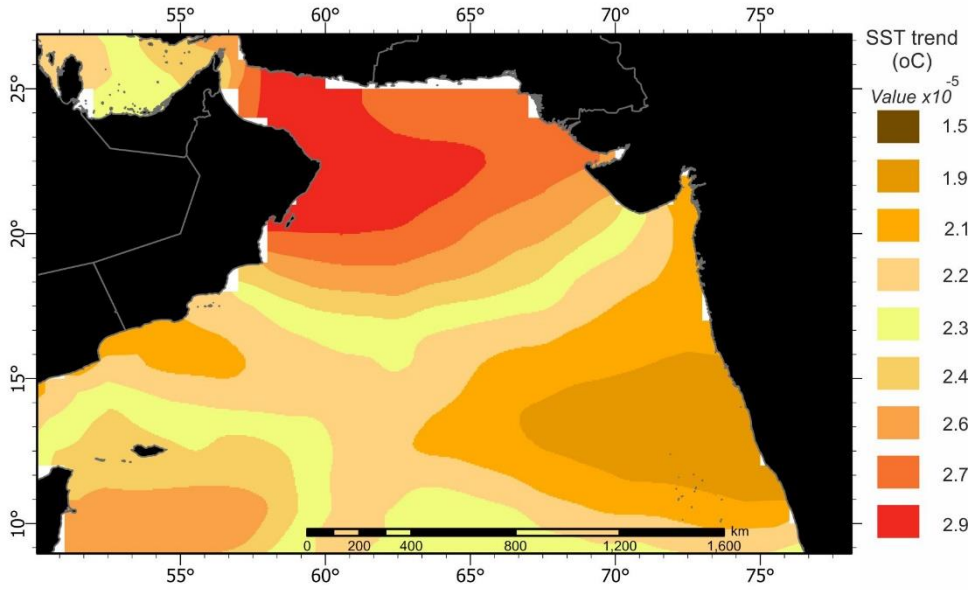


Figure 3: Long term SST linear model ( $R^2=0.8$ ) for the period 1900-2021. The maximum SST trend changes is observed in the Gulf of Oman, Ras al Hadd and the northern Arabian Sea. Minimum SST changes are recorded in the east of the Arabian Sea where the highest number of tropical storm and cyclone events are recorded.

#### 4.2. Role of ocean currents in the spatial distribution of Persian Gulf water

##### 4.2.1. Upwelling

The depth of Persian Gulf water outflow is controlled by the intensity of upwelling. During low wind stress, when upwelling is minimum, outflow water sinks into the Gulf of Oman at Ras al Hamra and moves to the east between two low salinity water layers (Fig 4A). With increased upwelling intensity, eastward migration of the Persian Gulf water is interrupted. The outflow water depth decreases and water salinity and density increases to 200 m depth between 58° and 59.25° E. Simultaneously, warm and saline water outflow occurs through shallow water (0-70 meter; Fig 4B). The dense saline water sinks into deeper water (250 meters) during weaker upwelling. Strong storm events lead to intense upwelling in the Gulf of Oman and consequently the outflow water is disconnected, with low salinity water reaching the surface. Meanwhile, the depth of the warm and saline water increases and low salinity water lenses emerge between the saline masses (Fig 4C).

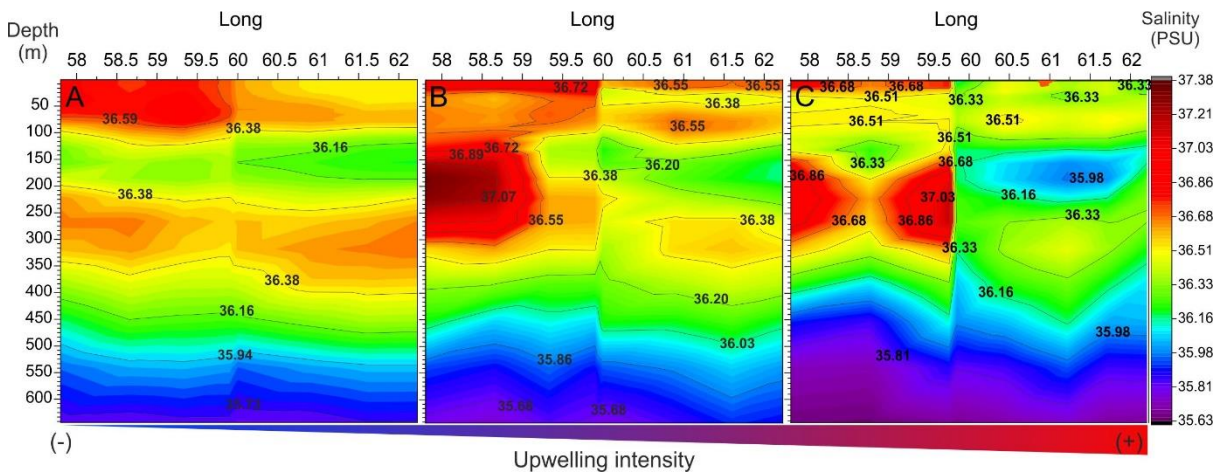


Figure 4: Salinity profile from the Gulf of Oman to the Arabian Sea during January to June 2010. A, B and C represent the Persian Gulf outflow water for weak, normal and intense upwelling intensities.

The long-term salinity and temperature profiles at Ras al Hamra for the period 1993 to 2020 show an increasing trend of the Persian Gulf outflow water depth. This event has been controlled by three

processes, (i) an increase in the salinity and the temperature of Persian Gulf water, (ii) an acceleration in the number of normal upwelling events in the Arabian Sea due to increasing wind speed and (iii) intense upwelling during strong storms. Maximum saline water depths are observed between 0-50 m and 150-300 m. The saline water (salinity > 36.5 PSU) was disconnected by low salinity water (salinity < 36.3 PSU) masses during upwelling processes. For the period 1993-2000, the maximum depth of Persian Gulf water was 230m. During this time interval, the upwelling water covered the saline mass and attained 15 m depth. The depth and volume of Persian Gulf water outflow has increased since 2000. Between 2000 and 2020, the depth of warm and saline outflow increased and attained a depth of 400 m in 2007. Since 2007, the depth of Persian Gulf water outflow has oscillated between 400-450 m due to intense upwelling events. Concurrently, the salinity and temperature of the outflow water has increased (Fig 5).

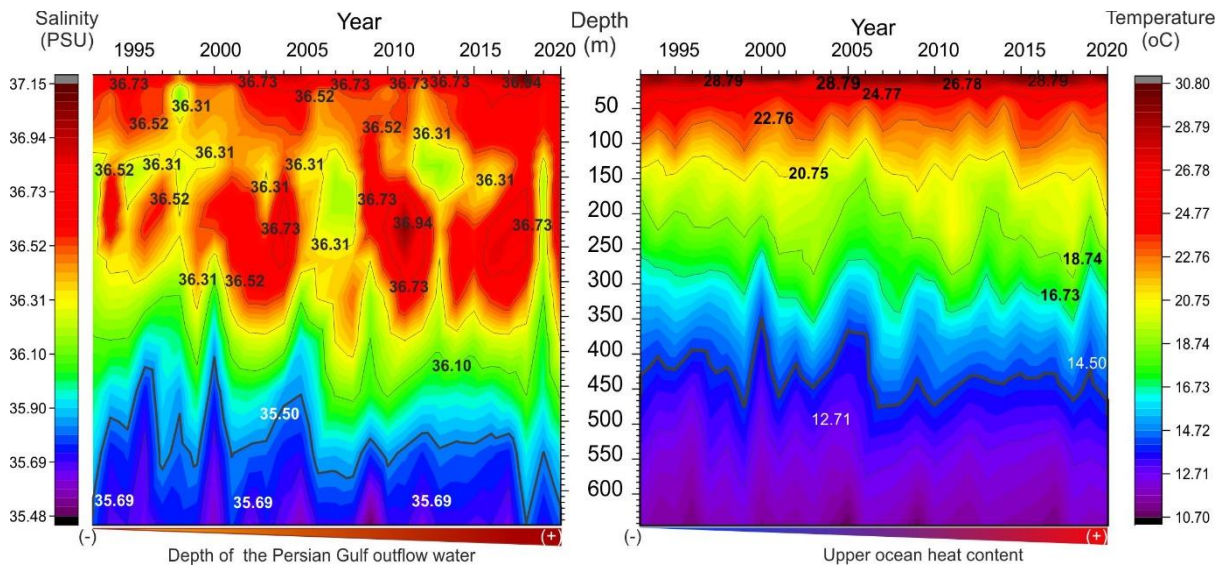


Figure 5: long-term salinity and temperature profiles at Ras al Hadd for the period 1993-2020.

#### 4.2.2 Eddy currents and the Ras al Hadd dipole jet

Mesoscale features such as eddies and jets in the Gulf of Oman and the Arabian Sea have significant impacts on the distribution of Persian Gulf outflow and upper ocean heat content changes. The eddy intensity in the western part of Arabian Sea is controlled by wind stress and dipole jets. The cyclonic eddies are associated with upwelling with low surface anomaly and anticyclonic eddies which are associated with downwelling and high sea surface anomalies. The temperature of the eddy cores is controlled by sea water temperature at the surface and in deeper layers. The cyclonic eddy north and west of the Arabian Sea is generally shallow and the cores' temperature depends on upwelling and the Persian Gulf water depth. As a result, the shallow Persian Gulf outflow and heat advection by dipole jets have significant impacts on the core temperature and salinity of cyclonic eddies. The cyclonic eddies which are under the influence of Persian Gulf water have warm and saline cores, while warm cores with lower salinity are observed around the dipole jets.

The intensity of anticyclonic eddies at Ras al Hadd is controlled by wind stress and the intensity of dipole jets. The temperature and salinity of the eddy cores are controlled by water temperature in the Gulf of Oman and upwelling processes. During normal upwelling, salinity and temperature at the eddy core increases via low depth outflow water. The increased depth of the outflow water at Ras al Hamra during intense upwelling leads to a decrease in temperature at the anticyclonic eddy core. A cold eddy core occurs when cold upwelling water reaches the surface in the Gulf of Oman. Increasing wind stress in the west of the Arabian Sea lead to accelerating east Arabian currents and Ras al Hadd jet intensity. Consequently, Ekman pumping increases at Ras al Hadd. Shallow outflow resumes, leading to

decreasing wind stress and jet intensity, and therefore an increase in the eddy core temperature and salinity (Fig 6; see Fig A2).

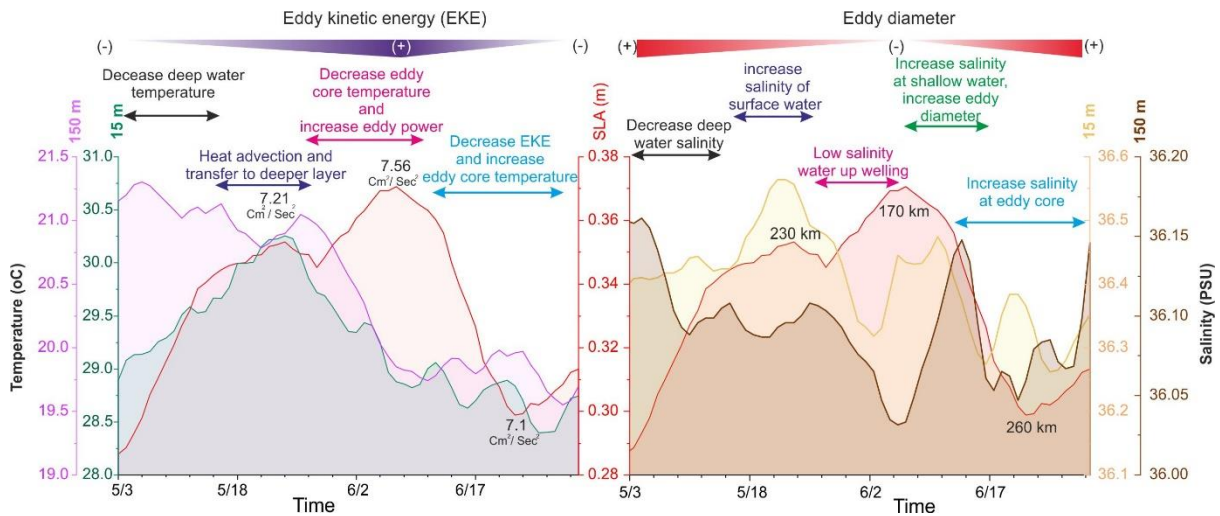


Figure 6: Anticyclonic eddy intensity changes at Ras al Hadd between May to June 2010. Cold water upwelling in early May lead to a decrease in water temperature and salinity at depths of 15 and 150 m. With increased upwelling and Ras al Hadd jet intensity, Ekman pumping increases and salinity and temperature increase at the eddy core. Temperature and salinity decrease at the eddy core due to enhanced upwelling and increased eddy power. With decreased wind stress, the eddy core temperature and salinity increase due to the Persian Gulf shallow outflow at Ras al Hadd.

### 4.3. Tropical cyclones

#### 4.2.1. Tropical cyclone Gonu

2007 was a La Niña year with neutral IOD. During May, northern Arabian Sea was influenced by a monsoon surge and active Madden-Julian Oscillation (MJO). Increased wind stress led to an intensification of anticyclonic eddies with warm cores in the Gulf of Oman and Ras al Hadd with 0.2 and 0.37m SLA, respectively. The Ras al Hadd jet speed was 0.38 m/s and Ekman Kinetic energy (EKE) attained  $7.62 \text{ cm}^2/\text{sec}^2$  (see Fig A3). The Persian Gulf warm and saline water was distributed along the Iranian and Pakistani coasts and transported to shallow water in the Arabian Sea (Fig 7).

On the 31<sup>st</sup> May, the monsoon surge produced an area of low-pressure omega at  $0-8^\circ\text{N}$  and  $59-68^\circ\text{E}$  and a high-pressure zone extended to the north of the Arabian Sea ( $19-24^\circ\text{N}$  and  $59-68^\circ\text{E}$ ). A depression with 1492 geopotential height (gph) developed at  $11.6^\circ\text{N}$  and  $72.6^\circ\text{E}$  in 850 hPa (see Fig A4). Wind speed at this pressure level was  $<5 \text{ ms}^{-1}$ . Concurrently, the cyclonic system induced a core of 5848 gph at 500 hPa ( $8.2^\circ\text{N}$  and  $67.5^\circ\text{E}$ ) with  $15 \text{ ms}^{-1}$  wind speed. The genesis of tropical cyclone Gonu (TCG) occurred at  $13.7^\circ\text{N}$  and  $71.6^\circ\text{E}$  where the SST anomaly (SSTA) and Sea-level anomaly (SLA) were  $1.17^\circ\text{C}$  and  $0.13\text{m}$ , respectively. TC Gonu tracked to the northeast (33 km) and passed over a warm core anticyclonic eddy with  $1.22^\circ\text{C}$  SSTA and  $0.19\text{m}$  SLA. After tracking 256 km, Gonu reached a cyclonic eddy ( $0.03\text{m}$  and  $0.82^\circ\text{C}$ ) and it tracked 189km to the west at category 0 during 12 hours (table 1). TCG tracked 102 km to the north in 18 hours along a dual core anticyclonic eddy. Gonu's category increased whilst tracking to the north and it attained category 1 when it passed over a warm ( $1.2^\circ\text{C}$ ) and saline (36.52 PSU) cyclonic eddy with  $0.01\text{m}$  SLA at  $67.05^\circ\text{E}$  and  $16.45^\circ\text{N}$ . Meanwhile, the  $26.5^\circ\text{C}$  isotherm and isohaline depth (36.6 PSU) reached 70-80 m depth (Fig 8). Therefore, warm and salty water was upwelled by the shallow (surface-intensified) cyclonic eddy. Gonu tracked 163km to the northwest over a cyclonic eddy where water temperature and salinity increased along the TC path (36.75 PSU and  $1.22^\circ\text{C}$ ). The TC intensity increased dramatically and its category evolved from 1 to 4 during 24 hours (Fig 7).

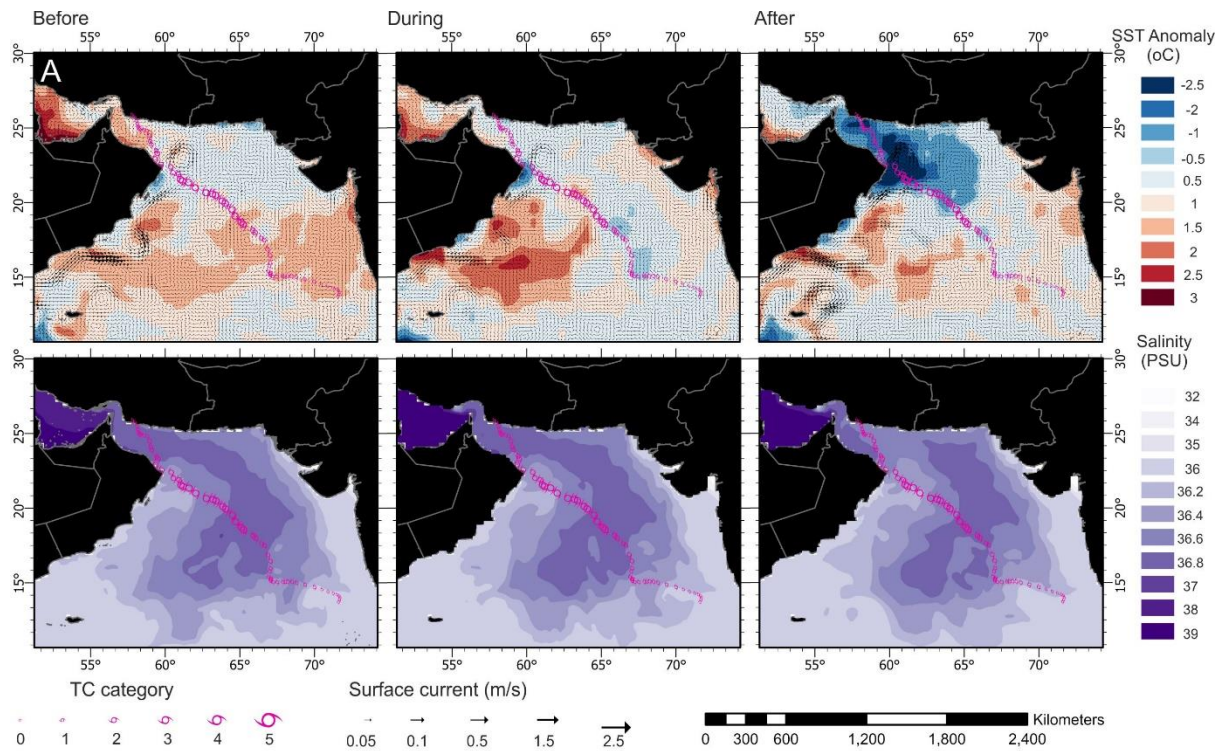


Figure 7: A) Sea Surface Temperature Anomaly (SSTA) and surface current changes before, during and after Gonu tropical cyclone (TCG). B) Mean salinity at shallow water (0-50m) for the mentioned periods. The high salinity water mass (36.6-36.8 PSU) areas are  $52.35 \times 10^4$ ,  $59.17 \times 10^4$  and  $40.92 \times 10^4 \text{ km}^2$  respectively for before, during and after Gonu. Gonu's track is depicted in purple.

In the course of TC intensification, east Arabian current speed attained 1m/s and SSTA in the west of the Arabian Sea reached  $2.18^\circ\text{C}$  through a cyclonic current with  $-0.05\text{m}$  SLA and 36.7 PSU at the core. Concurrently, cold water upwelling in the Oman upwelling zone increased and SSTA reached  $-2.8^\circ\text{C}$ , meanwhile, Ras al Hadd jet speed (0.58 m/s) and EKE ( $7.9 \text{ cm}^2/\text{sec}^2$ ) increased (see Fig A3). The Ras al Hadd jet intensification had significant impacts on northern anticyclonic eddy energy. The eddy current speed and SLA changed from 0.34 to 0.54 m/s and 0.36 to 0.37m, respectively. Increased upwelling at Ras al Hadd flowed into the Persian Gulf shallow water along the Iranian and Pakistani coasts. Therefore, the area of high saline water (36.6 to 37.8 PSU) increased by 11.43%. Wind stress increased due to the intensification of Gonu as it approached Ras al Hadd. Simultaneously, SSTA at the Ras al Hadd anticyclonic eddy core changed from  $0.79$  to  $0.12^\circ\text{C}$  due to intense cold water upwelling in the Gulf of Oman. Concurrent with widespread cooling in the Gulf of Oman, an increase in SSTA by up to  $0.79^\circ\text{C}$  occurred at the eastern end of Ras al Hadd jet, through an anticyclonic eddy.

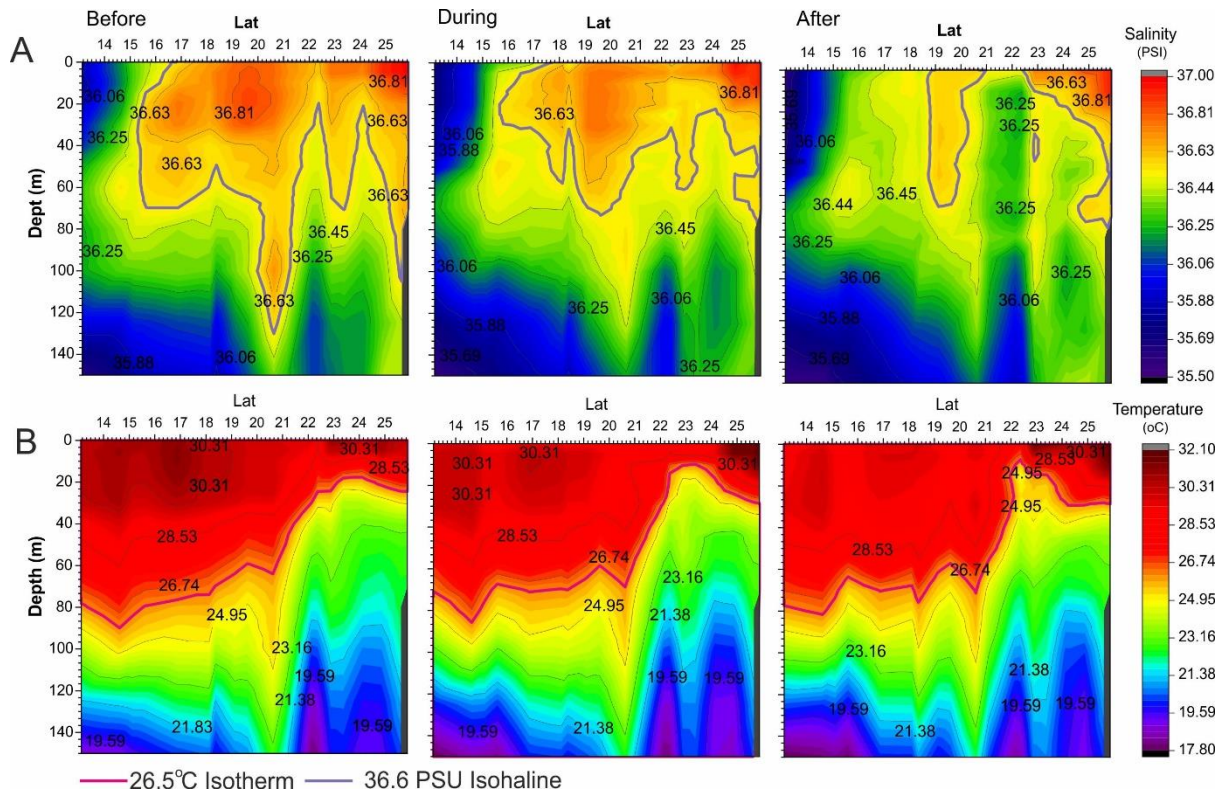


Figure 8: Salinity (A) and Temperature (B) profiles for tropical cyclone Gonu. The data were extracted from the location of the TC center before, during and after passage. The isohaline line for 36.6 evolved from 80 to 140 m. Maximum isohaline depth for 36.6 PSU is observed between 19 and 20°N. The upwelling zone is along 21.2 to 22.5 °N.

Between June 4<sup>th</sup> and 5<sup>th</sup>, the omega low-pressure cell shifted to the northeast and was located at 11.4°N and 61.3°E at both 850 and 500 hPa pressure levels. TC Gonu's column was well developed at both pressure levels (see Fig A4). By this time, the TC had tracked 189 km for 24 hours during which time it attained category 5 (table 1). Gonu reached to its maximum category when it cross over the anticyclonic eddy with the deepest haline stratification (36.6 isohaline depth reached to 125m, Fig 8). The TCG continued its track to the northwest where the 26.5 °C isotherm and isohaline (36.6 PSU) depth were decreased by approaching the upwelling zone (Fig 7). After tracking 205 km at category 4, the TC intensity decreased and tracked 87 km to the northwest at category 3. As Gonu continued to track to Ras al Hadd, the isotherm and isohaline water depth was decreased by intense upwelling. Gonu passed 3 km from Ras al Hadd and entered the Gulf of Oman at category 2 where the isotherm and isohaline depth were at 15 m depth. After 18 hours, the TC attained category zero and it made landfall on the Iranian coast (Jask). During Gonu's passage over the Gulf of Oman, cold water input into the Persian Gulf was increased and SST decreased along northern part of the Persian Gulf's central basin. Concurrently, Persian Gulf water outflow accelerated through the Strait of Hormuz. The high salinity water outflow (36.8 PSU) was redirected into deeper water (150-200m) at Ras al Hamra and the shallow highly saline water area decreased by 45% (Fig 7).

Table 1: Tropical cyclone Gonu 6 hourly ocean-atmospheric changes through the TCG core.

Coordination		Day	Hour	Category	SPL hPa	MJO Amplitude	SLA m	Salinity PSU	SSTA °C
LAT	LON								
13.7	71.6	31	6	-	-		0.13	35.72	0.98
14	71.7	31	12	-	-	1.81	0.15	35.73	1.18
14.2	71.5	31	18	-	-		0.16	35.85	1.17
14.4	70.9	1	0	-	-		0.19	36.02	1.22
14.7	70	1	6	-	-	1.55	0.18	35.96	1.20
15	68.8	1	12	-	-		0.06	36.41	0.99
15.08	68.24	1	18	-	1002		0.09	36.40	1.09
15.06	67.89	2	0	-	1002		0.12	36.36	1.12
15.05	67.23	2	6	0	-	1.71	0.10	36.27	1.74
15.2	67.05	2	12	0	992		0.17	36.26	1.56
15.3	67.1	2	18	0	992		0.17	36.35	1.56
15.75	67	3	0	0	988		0.18	36.35	1.64
16.45	67.05	3	6	0	988	1.75	0.19	36.50	1.75
17.5	66.65	3	12	1	988		0.17	36.59	1.42
18	66.05	3	18	1	980		0.11	36.60	1.05
18.55	65.25	4	0	2	974		0.08	36.61	1.29
19.1	64.7	4	6	4	952	1.65	0.09	36.62	1.35
19.95	64.05	4	12	4	934		0.15	36.71	1.35
20.5	63.4	4	18	5	920		0.23	36.55	0.84
20.65	62.75	5	0	5	936		0.15	36.54	0.98
21.35	61.6	5	6	4	950	1.60	0.17	36.52	0.91
21.55	61.05	5	12	4	960		0.14	36.27	-0.10
22	60.55	5	18	4	970		0.11	36.25	-0.12
22.55	59.75	6	0	3	970		0.10	36.25	-0.52
23.3	59.5	6	6	2	970	1.70	0.15	-	-2.61
23.9	59.1	6	12	2	970		0.11	36.54	-2.20
24.5	58.95	6	18	1	978		0.13	36.60	-2.50
24.87	58.6	7	0	1	988	1.78	0.16	36.56	-2.32
24.9	58.3	7	6	0	-		0.16	36.56	-2.37

#### 4.2.2. Tropical cyclone Phet

Tropical cyclone Phet (TCP) occurred between May 31<sup>st</sup> – June 7<sup>th</sup> 2010 during a La Niña year, negative IOD and active MJO. Increased westerly wind stress during a negative IOD phase led to widespread upwelling and an intensification of oceanographic currents (eddies and jets) in the western part of the Arabian Sea (Fig 9).

The salinity and temperature profiles along the cyclone track show that the 26.5°C isotherm in the center of the Arabian Sea reached 80 m depth and it decreased to the west and northwest when approaching the upwelling zone. The 36.6 PSU isohaline is observed in the center of the Arabian Sea (16.5 to 19°N) and the Gulf of Oman with a maximum depth of 35m (Fig 10). Two anticyclonic eddies in the Gulf of Oman and at Ras al Hadd redistributed the Persian Gulf water (37 PSU) via the Iranian and Pakistani coasts to the Arabian Sea (Fig 9).

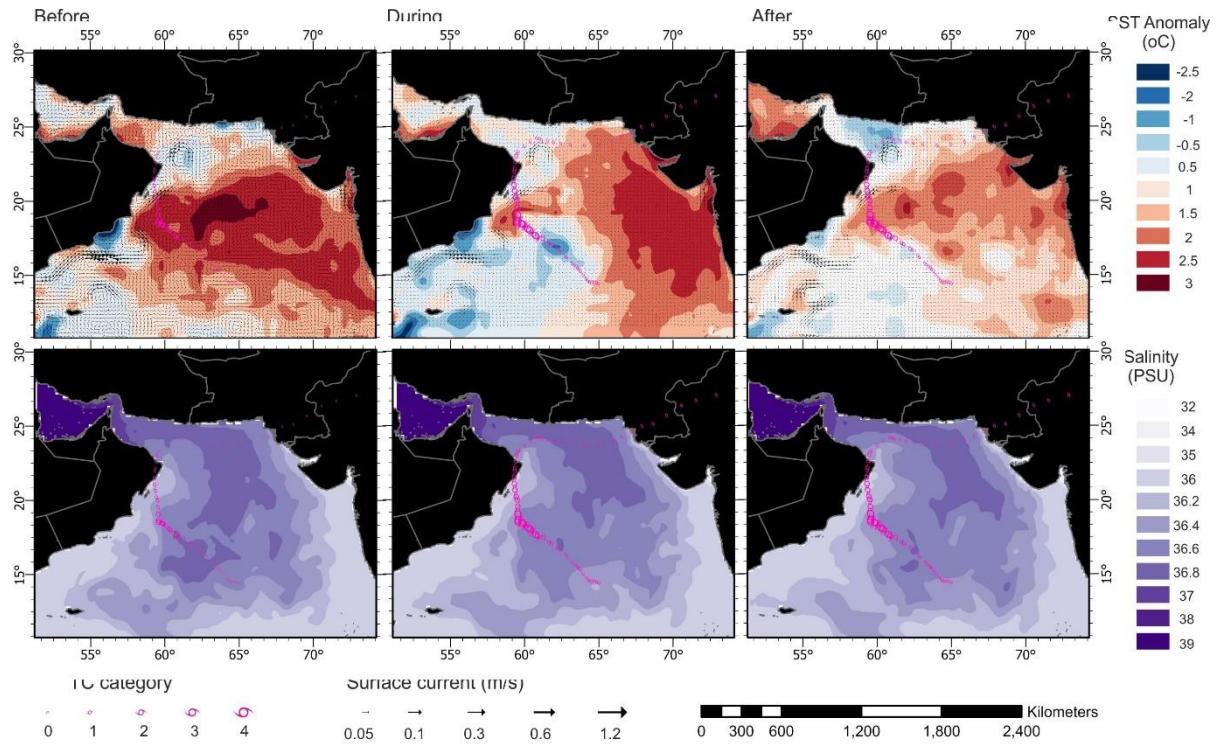


Figure 9: A) Sea Surface Temperature Anomaly (SSTA) and surface current changes for before, during and after Phet tropical cyclone (TCP). B) Mean salinity at shallow water depth (0-50 m) for the mentioned periods. The high salinity water mass (36.6-36.8 PSU) areas are  $45.22 \times 10^4$ ,  $35.35 \times 10^4$  and  $27.46 \times 10^4 \text{ km}^2$  respectively for before, during and after TCP. The water mass was discontinued in the center of the Arabian Sea. TC Phet's track is depicted in purple.

Increased wind stress in the western Arabian Sea during a negative IOD phase led to intensification of the eastern Arabian Sea current and the Ras al Hadd jet along the Oman coast and eddies in the center of the Arabian Sea (see Fig A5). SSTA increased in the west and the center of the Arabian Sea where the isotherm and isohaline reached their maximum depth. Heat advection and transportation occurred by shallow eddies and dipole jets. Meanwhile, intense upwelling decreased SSTA at the anticyclonic eddy at Ras al Hadd ( $-0.52^\circ\text{C}$ , SLA: 0.3m), coastal areas of Pakistan, Somalia and the southwest of the Oman. Therefore, SSTA and salinity values show a rising trend from the west (upwelling zone) to the center of the Arabian Sea (thick warm/saline stratification), evolving from 1.9 to  $3.12^\circ\text{C}$  and 35.77 to 36.73 PSU (Fig 9).

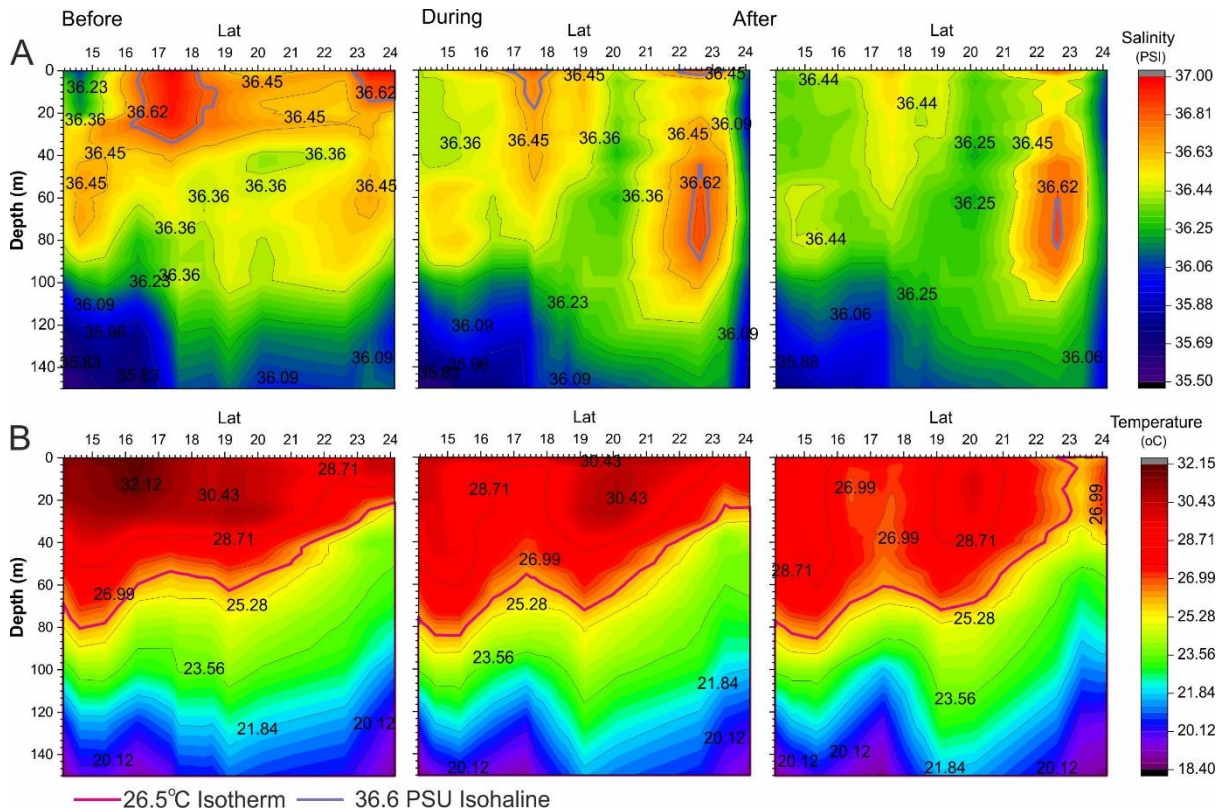


Figure 10: Salinity and temperature profiles along the tropical cyclone Phet's tracking path before, during and after the TC event. Isotherm (26.5 °C) depth decreased to the northwest on its approach to the upwelling zone. The isohaline (36.6 PSU) is not continuous and observed at the center of the Arabian Sea and southwest of the Gulf Oman with maximum depth of 35 m. With increased upwelling during the TC, the Isohaline depth increased at Ras al Hadd and it attained 80 m depth.

A monsoon surge occurred at the end of May producing widespread convection in the southeastern part of the Arabian Sea. A low-pressure system developed over the Arabian Sea, on the 30<sup>th</sup> May 2010. Meanwhile, a low-pressure omega extended to 10°N and 64°E at 850 and 500 hPa (see Fig A6). TCP formed at 14.4°N and 65°E over a warm core cyclonic eddy with 1.04°C SSTA and 0.06 m SLA. TCP started its track to the northwest as a tropical depression and after tracking 126 km it attained category zero by crossing over a warm (1.68°C) and saline (36.51 PSU) anticyclonic eddy with 0.22m SLA. The TC tracked 125 km to the northwest for 18 hours. Phet attained category 1 over an anticyclonic eddy with a very warm (2.11°C) and saline (36.73 PSU) core. The transition from TC category 1 to 4 was very rapid and occurred during a 10-hour period when it crossed over warm (2.13 °C) and saline water (36.8 PSU, Fig 9). TCP tracked 140 km to the northwest and its path shifted northwards at category 4.

EKE through the east Arabian current and Ras al Hadd jet were amplified (from 8.3 to 8.7 cm<sup>2</sup>/sec<sup>2</sup> and 7.4 to 7.7 cm<sup>2</sup>/sec<sup>2</sup>, respectively) by increasing wind stress. Therefore, the intensity of both the anticyclonic eddy to the north (EKE from 7.7 to 7.43 cm<sup>2</sup>/sec<sup>2</sup> and SLA from 0.36 to 0.37m) and south (EKE from 6.7 to 6.98 cm<sup>2</sup>/sec<sup>2</sup> and SLA from 0.29 to 0.31) of the Ras al Hadd jet increased. Increased eddy intensity led to rising SSTA in the northern eddy (Ras al Hadd) and SSTA attained 1°C at the eddy core. Concurrently, the Persian Gulf shallow water outflow decreased and the high salinity water area fell by 28%. Increased heat advection by geostrophic currents led to the expansion of a warm and low salinity water mass along the eastern coast of Oman (upwelling zone).

TC Phet's category decreased when it reached a low salinity and warm water mass and it tracked 190 km at category 3. The category decreased when approaching the Oman coast and it made landfall at category 2 on the east coast of Oman. Phet entered the Gulf of Oman at category 1 where the SSTA decreased due to the intense upwelling. Concurrently, the increased depth of the Persian Gulf outflow water led to a fall in the high salinity shallow water mass area in the Arabian Sea by 28.7% (Fig 9). A

cold core was observed for all anticyclonic eddies at Ras al Hadd and in the Gulf of Oman, consequently, for 3 hours the TC category attained zero. Phet tracked 170 km to the northeast before the path changed to the southeast and east. After tracking 680 km, it made a second landfall on the coast of Pakistan.

Table 2: Tropical cyclone Phet 6 hourly ocean-atmospheric changes through the TC core

Coordination		Day	Hour	Category	SLP	MJO	SLA	Salinity	SST
LAT	LON				hPa	Amplitude	M	PSU	°C
14.4	65	30	12	-	-	1.49	0.09	36.43	1.31
14.5	64.7	30	18	-	-		0.10	36.43	1.12
14.5	64.4	31	0	-	-		0.10	36.43	1.08
14.76	64.16	31	6	-	1001	1.48	0.16	36.47	1.17
15.21	63.79	31	12	-	1001		0.18	36.49	1.37
15.45	63.6	31	18	0	999		0.19	36.57	1.58
15.65	63.35	1	0	0	998		0.19	36.69	1.66
16.15	62.85	1	6	0	996	1.43	0.13	36.58	2.07
16.65	62.4	1	12	0	994		0.08	36.68	1.99
17.05	61.8	1	18	1	990		0.09	36.68	2.22
17.45	61.25	2	0	2	986		0.11	36.52	2.05
17.65	60.75	2	6	4	978	1.05	0.15	36.61	2.06
18.1	60.25	2	12	4	964		0.18	36.55	1.97
18.45	59.85	2	18	4	966		0.20	36.41	2.15
18.5	59.55	3	0	4	974		0.17	36.34	0.78
19.05	59.55	3	6	4	978	0.89	0.28	36.35	1.24
20	59.5	3	12	3	978		0.29	36.12	1.64
20.65	59.35	3	18	3	980		0.04	36.06	0.28
23.3	59.6	4	18	0	980	0.90	0.08	-	-0.58
23.95	60.4	5	0	0	990		0.09	36.37	-1.61
24.15	61	5	6	0	992	0.88	0.09	36.51	-1.78
24	61.55	5	12	0	992		0.09	36.52	-0.58
23.85	62.45	5	18	0	994		0.03	36.59	0.83
23.7	64.05	6	0	0	994		0.12	36.64	0.99
23.95	65.9	6	6	0	994	0.95	0.11	36.61	0.50
24.55	67.15	6	12	-	-		-	-	-
25.1	68.65	6	18	-	991		-	-	-
26.35	70.55	7	0	-	993	1.07	-	-	-
27.05	72.9	7	6	-	995		-	-	-

#### 4.2.3. Tropical cyclone Shaheen

Gulab and Shaheen were two related tropical cyclones that occurred during a La Niña and neutral IOD year with active MJO. Gulab cyclone formed in the Bay of Bengal between the 24<sup>th</sup> and 25<sup>th</sup> September 2021 and reached the Arabian Sea on the 29<sup>th</sup> September where two cyclonic eddies had already developed in the Gulf of Oman and in the northern Arabian Sea.

The cyclonic eddy in the Gulf of Oman modified the water distribution of the Persian Gulf. The warm and saline water outflow depth was decreased by Ekman suction and upwelling. Outflowing water was transported through the northern coast of Oman. The Persian Gulf water salinity decreased through the cyclonic geostrophic current and it changed from 37.5 PSU at Ras al Hamra to 36.83 PSU at Ras al Hadd. Meanwhile, SSTA values changed between 2.8 in the coastal zone and 2.27 offshore. Furthermore, SSTA and salinity decreased towards the cyclonic eddy core (1.2°C-36.72 PSU) and along the Iranian coast (0.39°C and 36.61 PSU; Fig 11).

The cyclonic eddy with -0.19m SLA at its core and 7.25 cm<sup>2</sup>/sec<sup>2</sup> EKE in the Gulf of Oman led to a decrease in the isohaline (36.6 PSU) depth to 20 m (Fig 12). A shallow warm and saline water

stratification was created in the Gulf of Oman (see Fig A7). The isohaline depth was increased with increasing distance from the eddy core and it became shallow towards the east. A dual core cyclonic eddy (0.006 and 0.004m SAL) prevented movement of the Persian Gulf water to the east. Therefore, two water stratifications were created in the north of the Arabian Sea. The first one is a low salinity warm water mass at 65° to 66°E that is under the influence of geostrophic currents and the second stratification was high salinity warm water located at 63.5° to 61°. The second water stratification was created by Persian Gulf water transport by the cyclonic current in the Gulf of Oman. The isohaline was at 70 m depth and the isotherm at 25 m depth. The isotherm depth increased to the east and it reached 30 m in the dual core eddy (Fig 12). The dual core eddy had warm and saline cores; salinity was higher in the southern core (36.73 PSU), while, temperature was higher in the northern core (2.03°C)

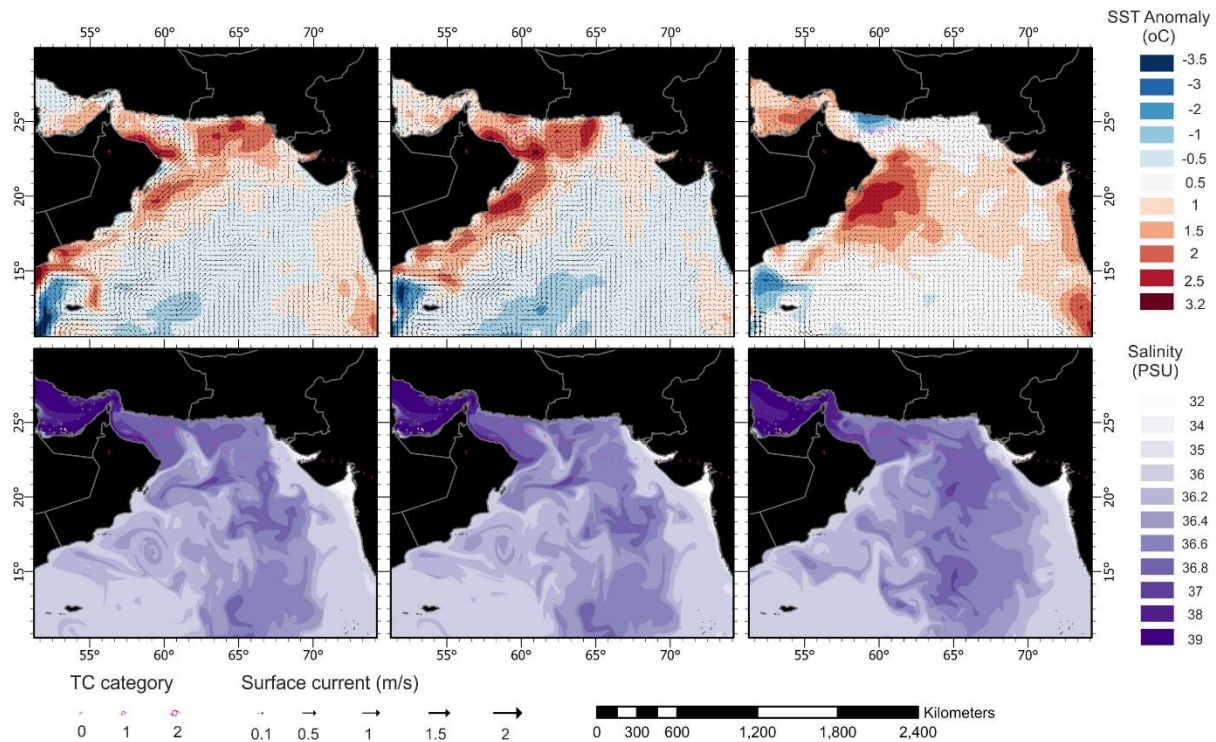


Figure 11: SSTA and surface current for before, during and after Shaheen tropical cyclone (TCS). B) Mean salinity at shallow water (0-50m) for the mentioned periods. Cyclonic eddies in the Gulf of Oman and the northern Arabian Sea prevented transportation of high-salinity water to the center of the Arabian Sea. After TCS and weakened eddy currents, Persian Gulf water moved to the Arabian Sea. The TCS track is depicted in purple color.

The cyclone Gulab became a low pressure system whilst crossing over India. On 30<sup>th</sup> September, a low-pressure omega developed at 22.5°N and 68°E and a depression was created at 850 hPa (see Fig A8); convection increased near the storm center (see Fig A9). Convection increased at the TC center on October 1<sup>st</sup> when it reached warm and saline water (1.03°C and 36.4 PSU, see Fig A9). Tropical cyclone Shaheen (TCS) attained category zero when SSTA and salinity attained 1.32°C and 36.6 PSU at 64.5-65°E. TCS intensity decreased again due to a fall in salinity (36.36-36.51 PSU) along the TCS track to the northwest. Salinity and temperature increased upon approaching the cyclonic eddy core. After tracking 196 km, the TCS attained category zero when it passed over warm and saline water (2°C and 36.6 PSU). The cyclone shifted to the west and became category 1 when crossing over a warm and high salinity water mass. When the TCS approached the Gulf of Oman, the cyclonic current in the Gulf of Oman was weakened and current speeds declined from 0.62 to 0.56m/s and EKE fell from 7.25 to 7 cm<sup>2</sup>/sec<sup>2</sup>. SSTA in the Gulf of Oman increased and it attained 1.47°C at the eddy core. Meanwhile, SSTA and salinity on the northern coast (2.2°C and 37 PSU) of Oman and at Ras al Hadd (2.54°C and 36.82 PSU) was enhanced. Warm and saline water was transported to the northwest along the TCS path. The TCS attained its maximum category when it crossed over the cyclonic eddy and it tracked 130 km

to the southwest (Fig 8). While tracking to the southwest, cold-water upwelling along the Iranian coast increased and SSTA on the Gulf of Oman decreased. Concurrently, heat advection was increased by the Ras al Hadd jets and eastern Arabian warm and low salinity water was transported to the west of the Arabian Sea. As a result, SSTA attained 2.27°C to the east of Oman. Finally, Shaheen made landfall over the northern Oman coast at category 1, making it the only cyclone to make landfall there since 1900.

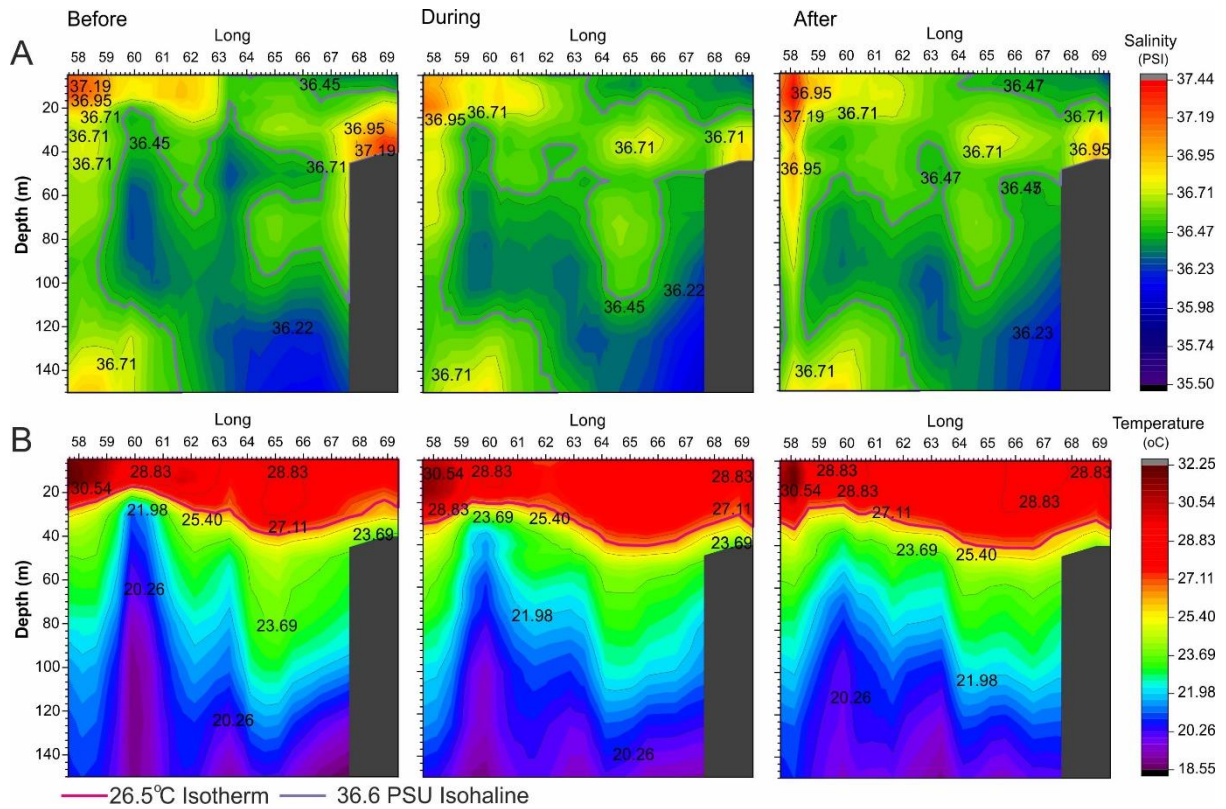


Figure 12: Salinity and temperature profiles (A and B) along the Shaheen tropical cyclone tracking path before, during and after the TC event. The isohaline and isotherm depth is controlled by the cyclonic eddy current in the Gulf of Oman and the Arabian Sea. 26.5°C depth increased from west to east and it became shallow through the cyclonic eddy. With weakening of the eddy currents and decreasing cold water upwelling, the depths of the isohaline and isotherm increased.

The TCS wind stress in the west of the Arabian Sea led to an increase in more intense surface eddy activities. Therefore, rising SSTA east of Oman continued through cyclonic and anticyclonic eddies. An increased warm (2.42°C) and low salinity (35.97 PSU) water mass to the east of Oman suggests that Ekman suction (shallow cyclonic eddy -0.05m SLA) was under the influence of the dipole jet transported water (Fig 11; see Fig A8).

Table 3: Tropical cyclone Shaheen 6 hourly category and translation speed changes

coordination		day	hour	Category	SLP	MJO	SLA	Salinity	SST
LAT	LON				hPa	amplitude	m	PSU	°C
22.43	71.31	29	12	-	1001		0.11	30.67	0.63
22.45	70.05	29	18	-	1002	1.44	0.10	33.42	0.61
22.5	68.9	30	0	-	1001		0.10	35.68	1.03
22.54	67.71	30	6	-	1002		0.08	36.48	1.37
22.57	66.58	30	12	-	997	1.67	0.09	36.54	1.17
22.64	65.55	30	18	-	994		0.13	36.44	1.27
22.8	64.7	1	0	0	992		0.12	36.53	1.34
23.09	64.07	1	6	-	990		0.04	36.71	1.71
23.47	63.59	1	12	-	982	1.74	0.05	36.73	1.98
23.9	63.2	1	18	1	981		0.11	30.67	0.63
23.9	62.5	2	0	1	981		0.06	36.58	1.85
24.1	61.6	2	6	1	983		0.11	36.04	1.58
24.5	60.7	2	12	2	978	1.76	0.02	36.35	1.00
24.3	60.1	2	18	2	977		-0.06	36.69	1.18
24.3	59.4	3	0	2	977		0.09	36.88	0.10
24.1	58.6	3	6	1	978		0.13	36.86	1.08
24	58.1	3	12	1	981	1.79	0.14	36.83	0.75
23.8	57.4	3	18	0	988		-	-	0.10

#### 4.4. Evaluation of tropical cyclone risks in the western Arabian Sea

The results of this study show that, in addition to large-scale atmospheric forcing, oceanographic currents and circulation have significantly affected TC strength in the Arabian Sea. Wind speed, SSTA and upper ocean heat content are the vital parameters for TC generation and salinity is important for tropical cyclone intensification. Long-term trend analysis and PCA score-axis 1 values are presented in Fig 13. Since 2000, 17 TCs (with a category greater than one) have occurred in the Arabian Sea. PCA-axis 1 shows 4 of them, which were influenced by water outflow from the Persian Gulf. TC risk associated with Persian Gulf outflow has increased dramatically since 2005, leading to increases in wind speed and upper ocean heat content in the north and west of the Arabian Sea during TC seasons. ARB 02 and Phet happened during La Niña and negative IOD years when upper ocean heat content manifests positive anomalies. Gonu and Shaheen occurred in La Niña and neutral IOD years when sea surface temperature in the Gulf of Oman was high and upper ocean heat content in eddy zones increased dramatically. Also, the temperature in the upwelling zone decreased due to increased wind speed. Finally, the peak in 2018 was related to the Mekunu TC that occurred during a neutral IOD and ENSO year (Fig 13). In 2018, we witness maximum upper ocean heat and wind speed in the north and west of the Arabian Sea, leading to an increase in sea surface temperature in the eddy and upwelling zone (Ras al Hadd jet intensification).

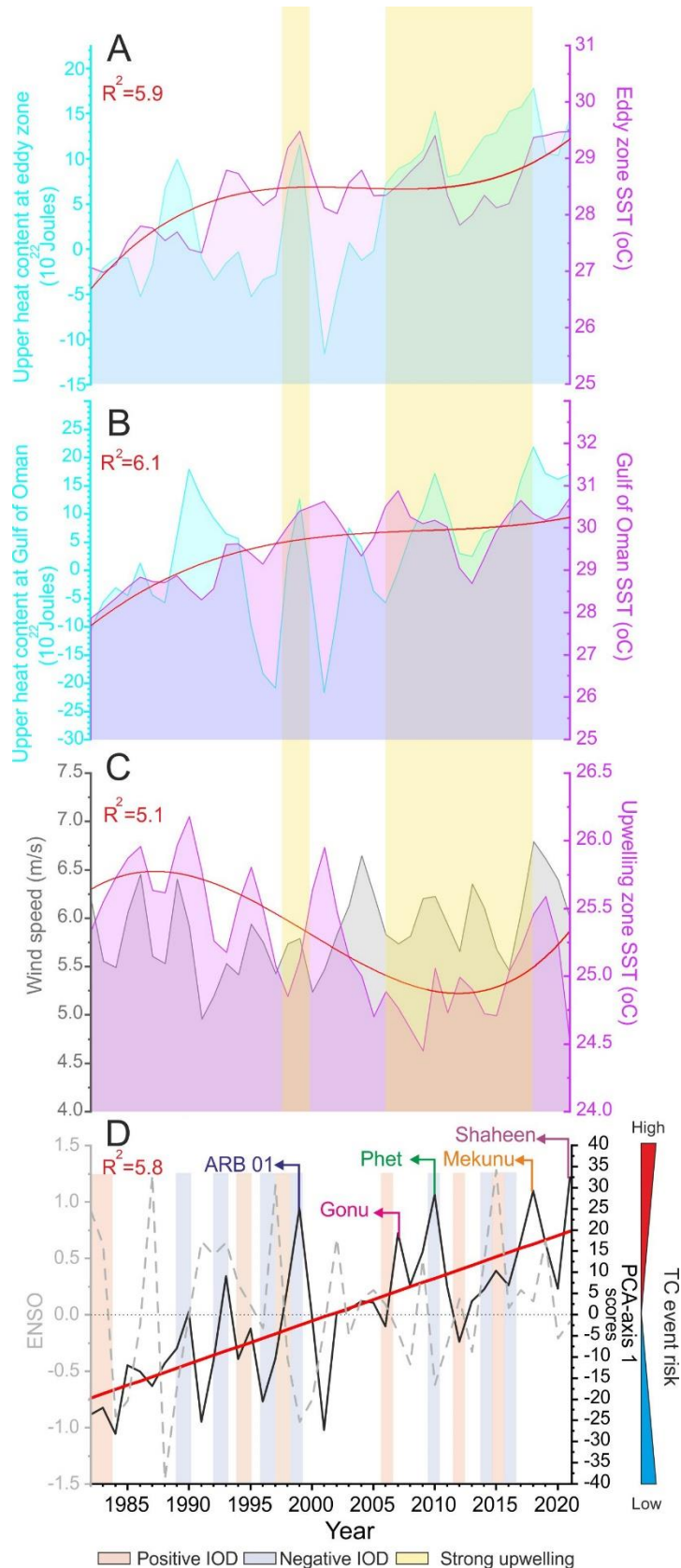


Figure 13: Tropical cyclone potential risks under the influence of the Persian Gulf water outflow for the north and west of the Arabian Sea. Long-term SST and upper ocean heat content trends for the tropical cyclone seasons are represented for (A) the eddy zones and (B) the Gulf of Oman. (C) Long-term SST and wind-speed changes for the Oman coast upwelling zone and (E) PCA-axis 1 (54% of total variance) are shown with the 95% confidence band. All the SSTA trends are highlighted by polynomial models (order 5,  $P_{value} < 0.001$ )

## 5. Discussion

Cold water upwelling in the western Arabian Sea is controlled by wind stress (Morrison, 1997; Joseph & Freeland, 2005). Long-term sea surface temperature (SST) analysis for the Arabian Sea demonstrates an increasing SST trend in the upwelling zones during the last 120 years. Increasing upper ocean heat content and heat transportation by Ras al Hadd jet and eastern Arabian currents are key factors in increasing SSTs in upwelling zones. SSTs also show increasing trends across the Arabian Sea; maximum temperatures are observed in the north and northwest, areas that are influenced by water outflow from the Persian Gulf.

A poleward migration of the monsoon jet axis and rising wind stress forces (Roxy et al. 2016; Aneesh and Sijikumar, 2016; Pratik et al., 2018) has led to a rise in southwest wind speeds since 1982 (Pourkerman et al., 2022) and an increased number of upwelling events in the Arabian Sea (Praveen et al., 2016). Rising upwelling events have created multiple branches for Persian Gulf outflow water and increasing salinity and temperature in shallow waters. Anticyclonic eddy currents in the Gulf of Oman and at Ras al Hadd have redistributed the shallow warm and saline water to the Arabian Sea along the Iranian and Pakistani coasts.

During the pre-monsoon and monsoon seasons, Persian Gulf water is transported to the Arabian Sea by ocean currents. The depth of the isohaline (36.6 PSU) and isotherm (26.5°C) in the center of the Arabian Sea is 80 m and it decreased towards the upwelling areas (west and northwest). Salinity and temperatures in surface water is controlled by the Persian Gulf outflow depth and eddy currents. Increased wind stress in the western Arabian Sea, in addition to enhanced upwelling and shallow water outflow, also increases eddies and jet intensities. Warm and saline water upwelling occurs through shallow Ekman suction and is transported to the anticyclonic eddy cores via geostrophic currents. Consequently, most of the eddies in the west and the center of the Arabian Sea have warm and saline cores during pre-monsoon seasons when advection occurs from the Persian Gulf water.

During post-monsoon seasons, concurrent with the domination of cyclonic eddies in the Gulf of Oman, warm and saline water transportation via the northern Arabian Sea is interrupted. Cold-water upwelling and deep cyclonic currents in the Gulf of Oman lead to Persian Gulf water outflow through multiple branches. There is an increase in salinity anomalies in deeper water (L'Hégare et al., 2013) and a short-term pause of outflow in surface waters along the northern Oman coast. Meanwhile, the Ras al Hadd dipole jet advects heat from the northern Oman coast and transports it to the west and southwest of the Arabian Sea. Heat transportation leads to domination of the warm eddy core with low salinity in the west of the Arabian Sea. Meanwhile, high salinity and a warm core eddy dominates the northern Arabian Sea. As a result, transportation of Persian Gulf water to the center of Arabian Sea is decreased.

Most tropical cyclones in the Arabian Sea occur during negative/neutral El Niño Southern Oscillation (ENSO) years and negative/neutral Indian Ocean dipole (IOD) phases. Higher rates of rapid TC intensification during La Niña years compared to El Niño years is related to high relative vorticity and anomalous low wind shear (Felton et al., 2013; Mahala et al., 2015; Bhardwaj et al., 2019). Meanwhile, during negative/neutral IOD phases, anomalously warm SSTs and high salinity water is created by the intensification of ocean currents (jets and eddies) that promote ocean/atmosphere conditions for TC formation and intensification.

Since 2000, the percentage of cyclones undergoing rapid intensification in the north Indian Ocean is 38% which is more than cyclones in the northern Pacific Ocean, which manifests a rate of 22% (Fudeyasu et al., 2018). The percentage of TC intensification in the Arabian Sea is greater than for the Bay of Bengal (Deshpande et al., 2021). Tropical cyclone intensification in the Arabian Sea has increased dramatically since 2007 and more than 72% of cyclones reached category 3 or more. This intensification has resulted from the creation of shallow warm and saline stratification due to the interaction between increasing wind stress in the west of the Arabian Sea and water outflow from the Persian Gulf. It creates favorable conditions for cyclones to obtain more energy and undergo

intensification (Balaguru et al. 2020; Fan et al., 2020). During the post-monsoon TC season, rapid intensification occurred in the center of the Arabian Sea where the maximum depth of the isohaline and isotherm existed. The TCs' intensity decreases dramatically to the west and north due to a decrease in water salinity and temperature. Instead, during the pre-monsoon TC season, tropical cyclone intensity increased to the north and northwest where the ocean currents provide the necessary warm and saline water for TC intensification. Tropical cyclone Shaheen is the only post-monsoon TC that made landfall on the northern Oman coast.

Increasing wind stress in the west of the Arabian Sea has led to increased upwelling events and the amplification of jets and Ras al Hadd anticyclonic intensities. During upwelling and Ekman pumping processes, temperature and salinity increased at depth. This process has accelerated, concurrent with the poleward migration of the summer monsoon belt since 2000. Meanwhile, pre-monsoon tropical cyclones have significant impacts on increasing temperature and salinity depths in the Gulf of Oman and the Arabian Sea. These cyclones, with a northwest direction increase anomalous wind stress in the west of the Arabian Sea. The TCs lead to (i) increasing ocean current (jets and eddies) and (ii) more intense upwelling in the Gulf of Oman. As a result, since 2007, in tandem with the onset of pre-monsoon TCs in the Arabian Sea, salinity and temperature depth have increased dramatically. Upper ocean heat content has grown in the Arabian Sea, increasing intense tropical cyclones during pre and post-monsoon seasons since 2007.

## **Conclusion**

Tropical cyclones constitute a new natural hazard for the people and governments of Iran, Pakistan and Oman. TC risks have increased dramatically since 2007 due to an increase in upper ocean heat content and salinity. The Persian Gulf water outflow is the main source of warm and saline water.

TC generation and intensity in the Arabian Sea has been controlled by Persian Gulf water outflow, which responds to ocean-atmospheric interactions. Increasing wind stress in the western Arabian Sea during pre-monsoon and monsoon seasons have led to an increase in Persian Gulf water outflow at shallow depths. The warm and saline water is transported to the center of the Arabian Sea via ocean currents. Meanwhile, during post-monsoon phases, high salinity and warm water have extended to the northern Arabian Sea and deeper water.

The most important parameters on the Persian Gulf water distribution are dipole jets and eddied currents at Ras al Hadd. During pre-monsoon and summer monsoon seasons, an anticyclonic eddy current at Ras al Hadd and in the Gulf of Oman transports warm and saline water to the center of the Arabian Sea via the Iranian and Pakistani coasts. Meanwhile, cyclonic eddy currents during post-monsoon seasons lead to increased salinity and temperature along the northern coast of Oman. Persian Gulf water transportation to the center of the Arabian Sea has been interrupted by Ras al Hadd jet and heat advection, and transported to the west and southwest via the jet.

Shallow Ekman suction (surface-intensified eddy) during the pre-monsoon seasons in the west and center of the Arabian Sea increase salinity and temperature in surface water due to the upwelling of Persian Gulf water. During post-monsoon seasons, cyclonic eddies in the northern Arabian Sea and the Gulf of Oman were influenced by Persian Gulf water, while, eddies that located in the center and west of the Arabian Sea lead to upwelling and high temperature and low salinity water.

Increasing wind stress and upwelling during the pre-monsoon seasons by negative/neutral IOD increases the potential risk of TC from a northwest direction (Phet and Gonu). Instead, the post-monsoon TCs affect the center and the southwest of the Arabian Sea. Generally, the post-monsoon TCs intensified in the center of the Arabian Sea and their intensity decreased when tracking to the north and northwest. Tropical cyclone Shaheen was the first post-monsoon TC in the northern Arabian Sea. It was a remnant of Cyclone Gulab, which re-intensified after reaching warm and saline water.

The frequency of strong TCs will increase in the next century due to global warming effects on the Persian Gulf, the Arabian Sea and the Gulf of Oman. Therefore mitigation plans via international platforms such as UNESCO and the IOI are necessary for at risk countries such as Iran, Oman and Pakistan to reduce infrastructural damage and the loss of human life caused by TC events.

## Acknowledgements

This study has been supported by Iran's National Elites Foundation (postdoctoral contract No. 101/70872). The Iranian National Institute for Oceanography and Atmospheric Sciences (INIO-AS) assisted with logistics.

## Data availability

All data is publicly available.

## Reference

- Ackerman, S. A., and J. A. Knox, (2015). *Meteorology: Understanding the Atmosphere*. 4th ed. Jones and Bartlett Learning, 575 pp.
- Aneesh, S., & Sijikumar, S. (2016). Changes in the south Asian monsoon low level jet during recent decades and its role in the monsoon water cycle. *Journal of Atmospheric and Solar-Terrestrial Physics*, 138, 47-53. <https://doi.org/10.1016/j.jastp.2015.12.009>
- Ayouche, A., De Marez, C., Morvan, M., L'Hegaret, P., Carton, X., Le Vu, B., & Stegner, A. (2021). Structure and Dynamics of the Ras al Hadd Oceanic Dipole in the Arabian Sea. *Oceans 2021*, 2, 105–125. <https://doi.org/10.3390/oceans2010007>
- Balaguru, K., Foltz, G. R., Leung, L. R., Kaplan, J., Xu, W., Reul, N., & Chapron, B. (2020). Pronounced impact of salinity on rapidly intensifying tropical cyclones. *Bulletin of the American Meteorological Society*, 101(9), E1497-E1511. <https://doi.org/10.1175/BAMS-D-19-0303.1>
- Bandyopadhyay, S., Dasgupta, S., Khan, Z. H., & Wheeler, D. (2021). Spatiotemporal Analysis of Tropical Cyclone Landfalls in Northern Bay of Bengal, India and Bangladesh. *Asia-Pacific Journal of Atmospheric Sciences*, 1-17. <https://doi.org/10.1007/s13143-021-00236-3>
- Bennani, Y., Ayouche, A., & Carton, X. (2022). 3D Structure of the Ras Al Hadd Oceanic Dipole. *Oceans 3*(3), 268-288. <https://doi.org/10.3390/oceans3030019>
- Bhardwaj, P., Pattanaik, D. R., & Singh, O. (2019). Tropical cyclone activity over Bay of Bengal in relation to El Niño-Southern Oscillation. *International Journal of Climatology*, 39(14), 5452-5469. <https://doi.org/10.1002/joc.6165>.
- Böhm, E., Morrison, J. M., Manghnani, V., Kim, H. S., & Flagg, C. N. (1999). The Ras al Hadd Jet: remotely sensed and acoustic Doppler current profiler observations in 1994–1995. *Deep Sea Research Part II: Topical Studies in Oceanography*, 46(8-9), 1531-1549. [https://doi.org/10.1016/S0967-0645\(99\)00034-X](https://doi.org/10.1016/S0967-0645(99)00034-X)
- Brandt, P., Stramma, L., Schott, F., Fischer, J., Dengler, M., & Quadfasel, D. (2002). Annual Rossby waves in the Arabian Sea from TOPEX/POSEIDON altimeter and in situ data. *Deep Sea Research Part II: Topical Studies in Oceanography*, 49(7-8), 1197-1210. [https://doi.org/10.1016/S0967-0645\(01\)00166-7](https://doi.org/10.1016/S0967-0645(01)00166-7)
- Cheng, Y. H., Ho, C. R., Zheng, Q., & Kuo, N. J. (2014). Statistical characteristics of mesoscale eddies in the North Pacific derived from satellite altimetry. *Remote Sensing*, 6(6), 5164-5183. <https://doi.org/10.3390/rs6065164>
- Deshpande, M., Singh, V. K., Ganadhi, M. K., Roxy, M. K., Emmanuel, R., & Kumar, U. (2021). Changing status of tropical cyclones over the north Indian Ocean. *Climate Dynamics*, 57(11), 3545-3567. <https://doi.org/10.1007/s00382-021-05880-z>
- Dong, C., McWilliams, J. C., Liu, Y., & Chen, D. (2014). Global heat and salt transports by eddy movement. *Nature communications*, 5(1), 1-6. <https://doi.org/10.1038/ncomms4294>
- Emanuel, K., DesAutels, C., Holloway, C., & Korty, R. (2004). Environmental control of tropical cyclone intensity. *Journal of the atmospheric sciences*, 61(7), 843-858. [https://doi.org/10.1175/1520-0469\(2004\)061<0843:ECOTCI>2.0.CO;2](https://doi.org/10.1175/1520-0469(2004)061<0843:ECOTCI>2.0.CO;2)
- Fan, K., Wang, X., & He, Z. (2020). Control of salinity stratification on recent increase in tropical cyclone intensification rates over the postmonsoon Bay of Bengal. *Environmental Research Letters*, 15(9), 094028. <https://doi.org/10.1088/1748-9326/ab9690>
- Felton, C. S., Subrahmanyam, B., & Murty, V. S. N. (2013). ENSO-modulated cyclogenesis over the Bay of Bengal. *Journal of Climate*, 26(24), 9806-9818. <https://doi.org/10.1175/JCLI-D-13-00134.1>

Fudeyasu, H., Ito, K., Miyamoto, Y., 2018. Characteristics of tropical cyclone rapid intensification over the Western North Pacific. *J. Clim.* 31, 8917–8930. <https://doi.org/10.1175/JCLI-D-17-0653.1>

Girishkumar, M. S., Suprit, K., Chiranjivi, J., Udaya Bhaskar, T. V. S., Ravichandran, M., Shesu, R. V., & Pattabhi Rama Rao, E. (2014). Observed oceanic response to tropical cyclone Jal from a moored buoy in the south-western Bay of Bengal. *Ocean Dynamics*, 64(3), 325-335. <https://doi.org/10.1007/s10236-014-0689-6>

Gray, W. M. (1979). Hurricanes: Their formation, structure and likely role in the tropical circulation. *Meteorology over the tropical oceans*, 155, 218.

Guinehut, S., Dhomps, A. L., Larnicol, G., & Le Traon, P. Y. (2012). High resolution 3-D temperature and salinity fields derived from in situ and satellite observations. *Ocean Science*, 8(5), 845-857. <https://doi.org/10.5194/os-8-845-2012>

Han, G., Ma, Z., Chen, D., Deyoung, B., & Chen, N. (2012). Observing storm surges from space: Hurricane Igor off Newfoundland. *Scientific reports*, 2(1), 1-9. <https://doi.org/10.1038/srep01010>

Huang, B., Liu, C., Banzon, V., Freeman, E., Graham, G., Hankins, B., ... & Zhang, H. M. (2021). Improvements of the daily optimum interpolation sea surface temperature (DOISST) version 2.1. *Journal of Climate*, 34(8), 2923-2939. <https://doi.org/10.1175/JCLI-D-20-0166.1>

Jangir, B., Swain, D., & Ghose, S. K. (2021). Influence of eddies and tropical cyclone heat potential on intensity changes of tropical cyclones in the North Indian Ocean. *Advances in Space Research*, 68(2), 773-786. <https://doi.org/10.1016/j.asr.2020.01.011>.

Johns, W. E., Yao, F., Olson, D. B., Josey, S. A., Grist, J. P., & Smeed, D. A. (2003). Observations of seasonal exchange through the Straits of Hormuz and the inferred heat and freshwater budgets of the Persian Gulf. *Journal of Geophysical Research: Oceans*, 108(C12). <https://doi.org/10.1029/2003JC001881>

Joseph, S., & Freeland, H. J. (2005). Salinity variability in the Arabian Sea. *Geophysical Research Letters*, 32, L09607. <https://doi.org/10.1029/2005GL022972>

Kawamura, R., Murakami, T., & Wang, B. (1996). Tropical and mid-latitude 45-day perturbations over the western Pacific during the northern summer. *Journal of the Meteorological Society of Japan. Ser. II*, 74(6), 867-890. [https://doi.org/10.2151/jmsj1965.74.6\\_867](https://doi.org/10.2151/jmsj1965.74.6_867)

Knapp, K. R., Kruk, M. C., Levinson, D. H., Diamond, H. J., & Neumann, C. J. (2010). The international best track archive for climate stewardship (IBTrACS) unifying tropical cyclone data. *Bulletin of the American Meteorological Society*, 91(3), 363-376. <https://doi.org/10.1175/2009BAMS2755.1>

Kumar, B., & Chakraborty, A. (2011). Movement of seasonal eddies and its relation with cyclonic heat potential and cyclogenesis points in the Bay of Bengal. *Natural hazards*, 59(3), 1671-1689. <https://doi.org/10.1007/s11069-011-9858-9>

Kurien, P., Ikeda, M., & Valsala, V. K. (2010). Mesoscale variability along the east coast of India in spring as revealed from satellite data and OGCM simulations. *Journal of oceanography*, 66(2), 273-289. <https://doi.org/10.1007/s10872-010-0024-x>.

L'Hégaret, P., Lacour, L., Carton, X., Rouillet, G., Baraille, R., & Corréard, S. (2013). A seasonal dipolar eddy near Ras Al Hamra (Sea of Oman). *Ocean Dynamics*, 63(6), 633-659. <https://doi.org/10.1007/s10236-013-0616-2>

Lavender, S. L., Hoeke, R. K., & Abbs, D. J. (2018). The influence of sea surface temperature on the intensity and associated storm surge of tropical cyclone Yasi: a sensitivity study. *Natural Hazards and Earth System Sciences*, 18(3), 795-805. <https://doi.org/10.5194/nhess-18-795-2018>

Li, Z., Li, T., Yu, W., Li, K., & Liu, Y. (2016). What controls the interannual variation of tropical cyclone genesis frequency over Bay of Bengal in the post-monsoon peak season?. *Atmospheric Science Letters*, 17(2), 148-154. <https://doi.org/10.1002/asl.636>.

Lorenz, M., Klingbeil, K., & Burchard, H. (2020). Numerical study of the exchange flow of the Persian Gulf using an extended total exchange flow analysis framework. *Journal of Geophysical Research: Oceans*, 125(2), e2019JC015527. <https://doi.org/10.1029/2019JC015527>

Lumpkin, R. (2016). Global characteristics of coherent vortices from surface drifter trajectories. *Journal of Geophysical Research: Oceans*, 121(2), 1306-1321. <https://doi.org/10.1002/2015JC011435>

Macdonald, A. M., & Wunsch, C. (1996). An estimate of global ocean circulation and heat fluxes. *Nature*, 382(6590), 436-439. <https://doi.org/10.1038/382436a0>

Mahala, B. K., Nayak, B. K., & Mohanty, P. K. (2015). Impacts of ENSO and IOD on tropical cyclone activity in the Bay of Bengal. *Natural Hazards*, 75(2), 1105-1125. <https://doi.org/10.1007/s11069-014-1360-8>

Mei, W., Xie, S. P., Primeau, F., McWilliams, J. C., & Pasquero, C. (2015). Northwestern Pacific typhoon intensity controlled by changes in ocean temperatures. *Science advances*, 1(4), e1500014. <https://doi.org/10.1126/sciadv.1500014>

Morrison, J. M. (1997). Inter-monsoonal changes in the T-S properties of the near-surface waters of the northern Arabian Sea. *Geophysical Research Letters*, 24, 2553–2556. <https://doi.org/10.1029/97GL01876>

- Mulet, S., Rio, M. H., Mignot, A., Guinehut, S., & Morrow, R. (2012). A new estimate of the global 3D geostrophic ocean circulation based on satellite data and in-situ measurements. *Deep Sea Research Part II: Topical Studies in Oceanography*, 77, 70-81. <https://doi.org/10.1016/j.dsr2.2012.04.012>
- Neumann, C. J. (1993). Global Overview, Chapter 1 Global Guide to Tropical Cyclone Forecasting, WMO. TC, (560).
- Palmén, E. (1948). On the formation and structure of tropical hurricanes. *Geophysica*, 3(1), 26-38.
- Pous, S. P., Carton, X., & Lazure, P. (2004b). Hydrology and circulation in the Strait of Hormuz and the Gulf of Oman—Results from the GOGP99 Experiment: 2. Gulf of Oman. *Journal of Geophysical Research: Oceans*, 109(C12). <https://doi.org/10.1029/2003JC002146>
- Pous, S., Carton, X. J., & Lazure, P. (2013). A process study of the wind-induced circulation in the Persian Gulf. *Open Journal of Marine Science*, 3(1), 27160. <https://doi.org/10.4236/ojms.2013.31001>
- Pratik, K., Parekh, A., Karmakar, A., Chowdary, J. S., & Gnanaseelan, C. (2019). Recent changes in the summer monsoon circulation and their impact on dynamics and thermodynamics of the Arabian Sea. *Theoretical and Applied Climatology*, 136(1), 321-331. <https://doi.org/10.1007/s00704-018-2493-6>
- Praveen, V., Ajayamohan, R. S., Valsala, V., & Sandeep, S. (2016). Intensification of upwelling along Oman coast in a warming scenario. *Geophysical Research Letters*, 43(14), 7581-7589. <https://doi.org/10.1002/2016GL069638>
- Reynolds, R. W., Smith, T. M., Liu, C., Chelton, D. B., Casey, K. S., & Schlax, M. G. (2007). Daily high-resolution-blended analyses for sea surface temperature. *Journal of climate*, 20(22), 5473-5496. <https://doi.org/10.1175/2007JCLI1824.1>
- Rouillet, G., Capet, X., & Maze, G. (2014). Global interior eddy available potential energy diagnosed from Argo floats. *Geophysical Research Letters*, 41(5), 1651-1656. <https://doi.org/10.1002/2013GL059004>
- Roxy, M. K., A. Modi, R. Murtugudde, V. Valsala, S. Panickal, S. P. Kumar, M. Ravichandran, M. Vichi, and M. Lévy (2016), A reduction in marine primary productivity driven by rapid warming over the tropical Indian Ocean, *Geophys. Res. Lett.*, 43, 826–833. <https://doi.org/10.1002/2015GL066979>
- Sandeep, S., & Ajayamohan, R. S. (2015). Poleward shift in Indian summer monsoon low level jetstream under global warming. *Climate Dynamics*, 45(1-2), 337-351. <https://doi.org/10.1007/s00382-014-2261-y>
- Scharffenberg, M. G., & Stammer, D. (2010). Seasonal variations of the large-scale geostrophic flow field and eddy kinetic energy inferred from the TOPEX/Poseidon and Jason-1 tandem mission data. *Journal of Geophysical Research: Oceans*, 115(C2). <https://doi.org/10.1029/2008JC005242>
- Shay, L. K., & Brewster, J. K. (2010). Oceanic heat content variability in the eastern Pacific Ocean for hurricane intensity forecasting. *Monthly Weather Review*, 138(6), 2110-2131. <https://doi.org/10.1175/2010MWR3189.1>
- Singh, O. P., Khan, T. M. A., & Rahman, M. S. (2001). Has the frequency of intense tropical cyclones increased in the north Indian Ocean?. *Current science*, 575-580.
- Singh, V. K., & Roxy, M. K. (2022). A review of ocean-atmosphere interactions during tropical cyclones in the north Indian Ocean. *Earth-Science Reviews*, 226, 103967. <https://doi.org/10.1016/j.earscirev.2022.103967>
- Singh, V. K., Roxy, M. K., & Deshpande, M. (2020). The unusual long track and rapid intensification of very severe cyclone Ockhi. *Curr. Sci*, 119(5), 771-779.
- Sun, J., Wang, D., Hu, X., Ling, Z., & Wang, L. (2019). Ongoing poleward migration of tropical cyclone occurrence over the western North Pacific Ocean. *Geophysical Research Letters*, 46(15), 9110-9117. <https://doi.org/10.1029/2019GL084260>
- Sun, J., Wang, G., Xiong, X., Hui, Z., Hu, X., Ling, Z.... & Chen, L. (2020). Impact of warm mesoscale eddy on tropical cyclone intensity. *Acta Oceanologica Sinica*, 39(8), 1-13. <https://doi.org/10.1007/s13131-020-1617-x>
- Sun, Y., Chen, C., Beardsley, R. C., Xu, Q., Qi, J., & Lin, H. (2013). Impact of current-wave interaction on storm surge simulation: A case study for Hurricane Bob. *Journal of Geophysical Research: Oceans*, 118(5), 2685-2701. <https://doi.org/10.1002/jgrc.20207>
- Trott, C. B., Subrahmanyam, B., & Murty, V. S. N. (2017). Variability of the Somali Current and eddies during the southwest monsoon regimes. *Dynamics of Atmospheres and Oceans*, 79, 43-55. <https://doi.org/10.1016/j.dynatmoce.2017.07.002>
- Trott, C. B., Subrahmanyam, B., Chaigneau, A., & Delcroix, T. (2018). Eddy tracking in the northwestern Indian Ocean during southwest monsoon regimes. *Geophysical Research Letters*, 45(13), 6594-6603. <https://doi.org/10.1029/2018GL078381>
- Vinayachandran, P. N., Kagimoto, T., Masumoto, Y., Chauhan, P., Nayak, S. R., & Yamagata, T. (2005). Bifurcation of the East India coastal current east of Sri Lanka. *Geophysical Research Letters*, 32(15). <https://doi.org/10.1029/2005GL022864>
- Wang, D. P., & Oey, L. Y. (2008). Hindcast of waves and currents in Hurricane Katrina. *Bulletin of the American Meteorological Society*, 89(4), 487-496. <https://doi.org/10.1175/BAMS-89-4-487>
- Xue, P., & Eltahir, E. A. (2015). Estimation of the heat and water budgets of the Persian (Arabian) Gulf using a regional climate model. *Journal of Climate*, 28(13), 5041-5062. <https://doi.org/10.1175/JCLI-D-14-00189.1>

Yablonsky, R. M., & Ginis, I. (2012). Impact of a warm ocean eddy's circulation on hurricane-induced sea surface cooling with implications for hurricane intensity. *Monthly Weather Review*, 141(3), 997-1021. <https://doi.org/10.1175/MWR-D-12-00248.1>

Yan, Y., Li, L., & Wang, C. (2017). The effects of oceanic barrier layer on the upper ocean response to tropical cyclones. *Journal of Geophysical Research: Oceans*, 122(6), 4829-4844. <https://doi: 10.1002/2017JC012694>

Yang, G., Yu, W., Yuan, Y., Zhao, X., Wang, F., Chen, G., ... & Duan, Y. (2015). Characteristics, vertical structures, and heat/salt transports of mesoscale eddies in the southeastern tropical Indian Ocean. *Journal of Geophysical Research: Oceans*, 120(10), 6733-6750. <https://doi: 10.1002/2015JC011130>

Zhan, P., Guo, D., & Hoteit, I. (2020). Eddy-Induced Transport and Kinetic Energy Budget in the Arabian Sea. *Geophysical Research Letters*, 47(23), e2020GL090490. . <https://doi10.1029/2020GL090490>

Zhang, H., Chen, D., Zhou, L., Liu, X., Ding, T., & Zhou, B. (2016). Upper ocean response to typhoon Kalmaegi (2014). *Journal of Geophysical Research: Oceans*, 121(8), 6520-6535. <https://doi.org/10.1002/2016JC012064>

Zhang, Z., Wang, W., & Qiu, B. (2014). Oceanic mass transport by mesoscale eddies. *Science*, 345(6194), 322-324. <https://doi.org/10.1126/science.1252418>